The Modulation of Daily Southern Africa Precipitation by El Niño–Southern Oscillation across the Summertime Wet Season

ANDREW HOELL,[a] ANDREA E. GAUGHAN,[b] TAMUKA MAGADZIRE,[c] AND LAURA HARRISON[d]

[a] *NOAA Physical Sciences Laboratory, Boulder, Colorado*
[b] *University of Louisville Department of Geography and Geosciences, Louisville, Kentucky*
[c] *Famine Early Warning Systems Network, Gaborone, Botswana*
[d] *Department of Geography, University of California Santa Barbara, Santa Barbara, California*

(Manuscript received 21 May 2020, in final form 15 September 2020)

ABSTRACT: The spatiotemporal evolution of daily southern Africa precipitation characteristics, and associated atmospheric circulation, related to El Niño and La Niña is examined across the region's November–April wet season. Precipitation characteristics are examined in terms of monthly changes in daily average precipitation, the number of precipitation days, and the number of heavy precipitation days in three independently constructed estimates of observed precipitation during 1983–2018. Mechanisms related to precipitation changes, including contributions from mass divergence, water vapor transports, and transient eddies, are diagnosed using the atmospheric moisture budget based on the ERA5 reanalysis. El Niño is related to precipitation anomalies that build during December–March, the core of the rainy season, culminating in significantly below average values stretching across a semiarid region from central Mozambique to southeastern Angola. A broad anticyclone centered over Botswana drives these precipitation anomalies primarily through anomalous mass divergence, with moisture advection and transient eddies playing secondary roles. La Niña is related to significantly above average daily precipitation characteristics over all Africa south of 20°S in February and much less so during the other five months. February precipitation anomalies are primarily driven through mass divergence due to a strong anomalous cyclonic circulation, whereas a similar circulation is more diffuse during the other months. The spatiotemporal evolutions of anomalies in daily precipitation characteristics across southern Africa related to El Niño and La Niña are not equal and opposite. The robustness of an asymmetric evolution, which could have implications for subseasonal forecasts, needs to be confirmed with analysis of additional empirical data and established with climate model experimentation.

KEYWORDS: Africa; Precipitation; El Niño; La Niña; Moisture/moisture budget

1. Introduction

Socioeconomic exposure to weather and climate is high in southern Africa (Fig. 1a) due to the region's reliance on predominantly rainfed agriculture and the demand for hydroelectric power (Conway et al. 2015). Rainfed agriculture employs up to 75% of the workforce and accounts for up to 50% of the southern Africa gross domestic product (Hulme 1996; Dixon et al. 2001) while hydropower provides almost 100% of the electricity to Lesotho, Malawi, and Zambia (Conway et al. 2015). The importance of the agricultural sector to southern African food security and economic prosperity is reinforced by African Union Commission initiatives and directly relates to agriculture-related United Nations Sustainable Development Goals (Nhemachena et al. 2018). Economic losses related to weather and climate extremes in southern Africa are costly (Niang et al. 2014): the gross domestic product during dry years is about 17% lower than wet years (Lindesay 1990) and the gross domestic product during 1983, among the driest years on record, was about 7% below average (Van Zyl et al. 1988). Given the environmental effects on socioeconomic growth in southern Africa (Jury 2002), a better understanding of how weather and climate modulate daily precipitation characteristics is of critical importance.

As a principal driver of southern Africa climate during the region's austral summer rainy season (e.g., Hastenrath et al. 1995; Manatsa et al. 2011), information on El Niño–Southern Oscillation (ENSO) has been applied to many economic sectors (Jury 2002; Smith and Ubilava 2017) to provide early warning of seasonal to annual extremes. ENSO was found to be a principal driver of seasonal climate based on average conditions across many El Niño and La Niña events (Figs. 1b,c; e.g., Nicholson and Entekhabi 1986; Ropelewski and Halpert 1987; Lindesay 1988; Jury et al. 1994; Rocha and Simmonds 1997; Nicholson and Kim 1997; Reason et al. 2000; Misra 2003; Manatsa et al. 2011). This research found that El Niño, the warm phase of ENSO, is related to below average precipitation on seasonal to annual time scales whereas La Niña, the cool phase of ENSO, is related to above average precipitation.

Dynamically, El Niño and La Niña events excite a midtropospheric convection dipole between the tropical west and central Pacific, which in turn excites circulation anomalies over southern Africa (Ratnam et al. 2014; Hoell et al. 2015). The anomalous circulations alter the vertical motions (Hoell et al. 2015) and moisture fluxes (Reason and Jagadheesha 2005; Hoell et al. 2015), which then force seasonal southern Africa precipitation anomalies. El Niño forces anomalous high pressure

Supplemental information related to this paper is available at the Journals Online website: https://doi.org/10.1175/JCLI-D-20-0379.s1.

Corresponding author: Andrew Hoell, andrew.hoell@noaa.gov

DOI: 10.1175/JCLI-D-20-0379.1

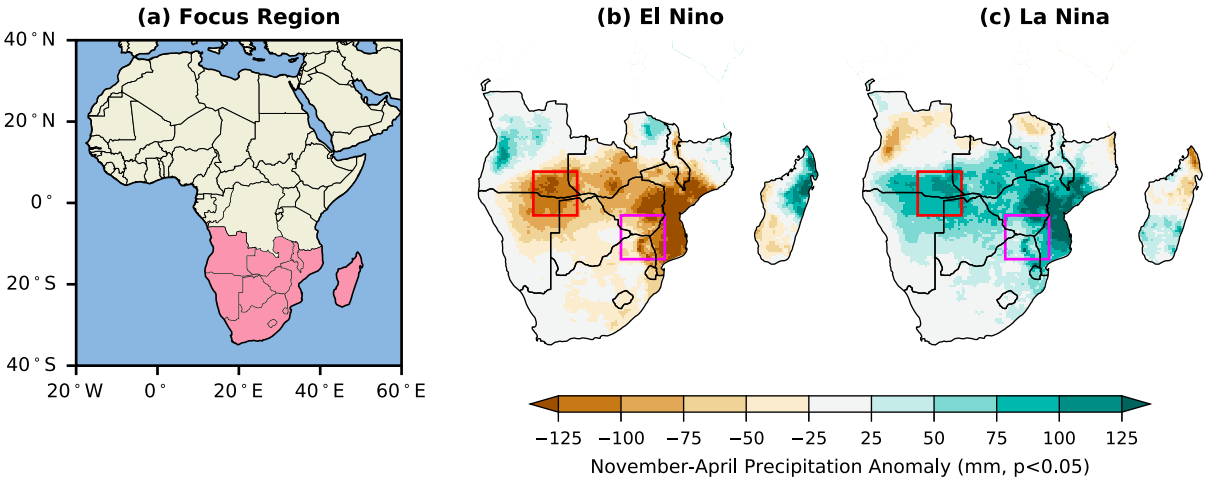

FIG. 1. (a) Southern Africa and November–April precipitation anomaly based on CHIRPS during (b) El Niño and (c) La Niña when December meets the criteria of a warm or cool ENSO event, respectively. The red and magenta rectangles in (b) and (c) denote the Longa–Mavinga and Limpopo regions, respectively, whose precipitation accumulations during ENSO events are shown in Fig. 2.

over southern Africa, which leads to reduced upward motion, moisture flux convergence, and precipitation over the region while La Niña forces anomalous low pressure over southern Africa, which leads to enhanced upward motion, moisture flux convergence, and precipitation over the region (Cook 2000, 2001; Hoell and Eischeid 2019).

Despite its utility, the established physical understanding for how ENSO affects seasonal southern Africa summertime climate has limitations. These limitations include informing the behavior of southern Africa weather and climate on subseasonal time scales and incorporating modulating influences by other factors on southern Africa climate during ENSO events. For the latter limitation, studies have found that southern Africa climate is strongly modulated by atmospheric variability from features like the Mozambique Channel trough (e.g., Lazenby et al. 2016; Barimalala et al. 2020) and the Angola low (e.g., Munday and Washington 2017; Howard and Washington 2018; Pascale et al. 2019; Crétat et al. 2019). For the Angola low, Blamey et al. (2018) found that precipitation during the 2015/16 rainy season, and especially October–December, was less than during El Niño events of similar magnitude, like 1982/83 and 1997/98, because the low was weak. Likewise, Reason and Jagadheesha (2005) and Lyon and Mason (2007, 2009) found that southern African precipitation during the 1997/98 wet season was not as far below average as was anticipated, despite the strong El Niño event, because the Angola low was unusually strong and farther south than average.

In addition, differences in southern Africa climate between ENSO events have also been attributed to differences in sea surface temperature (SST) anomalies in the Pacific and Indian Oceans. In the Pacific, the differences in the intensity and pattern of SST anomalies between El Niño or La Niña events (e.g., Wyrtki 1975; Capotondi et al. 2015) are related to different atmospheric circulations and southern Africa precipitation anomalies (e.g., Ratnam et al. 2014; Hoell et al. 2015; Pomposi et al. 2018; Gore et al. 2020). In the Indian Ocean, the subtropical Indian Ocean dipole (SIOD; Behera and Yamagata 2001; Reason 2001; Washington and Preston 2006) also modulates seasonal southern Africa precipitation during El Niño or La Niña events. The SIOD can complement or disrupt the forced ENSO response over southern Africa (Hoell et al. 2017a,b; Hoell and Chen 2018): when ENSO and SIOD are out of phase then the southern Africa response is stronger than if ENSO acted alone, but if ENSO and SIOD are in phase then the southern Africa response is weaker. A regional or seasonal link may exist between the Indian Ocean dipole mode (IOD; Saji et al. 1999) and southern Africa climate during ENSO events (Gaughan et al. 2016; Williams and Hanan 2011), although other studies find the relationship to be fleeting (Manatsa et al. 2011, 2012) or undetectable (Marchant et al. 2007; Hoell et al. 2017a; Pascale et al. 2019).

The established physical understanding for how ENSO affects seasonal southern Africa climate also cannot fully characterize the behavior of weather and climate on subseasonal time scales. To illustrate, Fig. 2 shows November–April daily precipitation accumulation during El Niño and La Niña events over the Limpopo and Longa–Mavinga regions of southern Africa (regions outlined in Fig. 1). These regions, both part of transfrontier conservation areas (Muboko 2017), were selected because they encompass vast national parks that are home to wildlife that attract a robust tourism industry and are home to rural communities highly dependent on rainfed agriculture. In agreement with previous studies, the seasonal and annual accumulation during La Niña years tends to be greater than during El Niño years. However, the daily precipitation characteristics across the rainy season are largely different between and among La Niña and El Niño years: precipitation days tend to be more frequent during La Niña, as is the occurrence of heavy rain days, and the traces of cumulative precipitation between La Niña and El Niño years separate in December, January, and February.

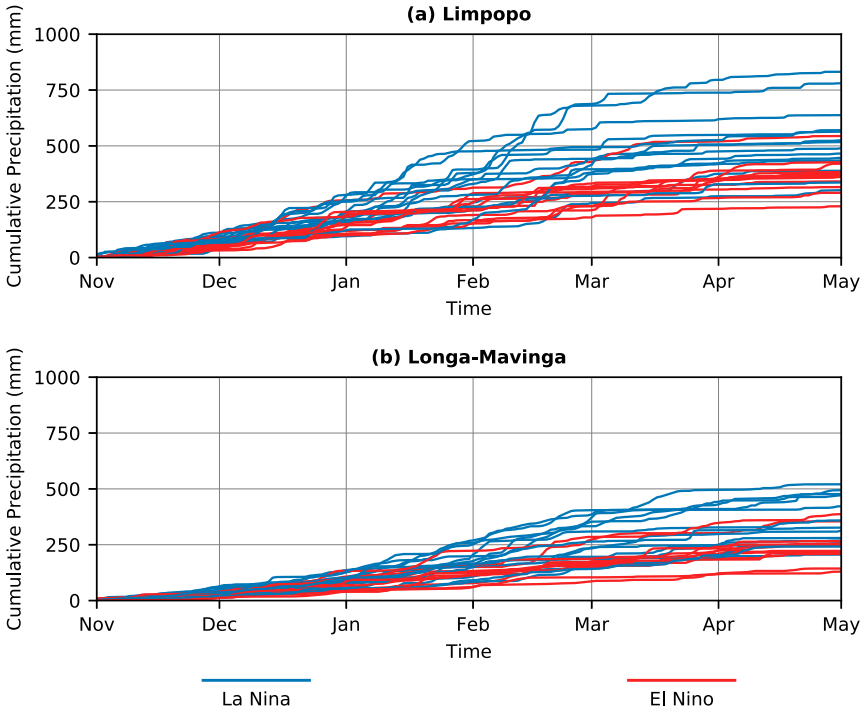

FIG. 2. Daily precipitation accumulation for (a) Limpopo and (b) Longa–Mavinga regions based on CHIRPS when December meets the criteria for La Niña (blue lines) and El Niño (red lines) events. The geographic location of the two regions is shown in Fig. 1.

Here, we examine daily precipitation characteristics related to El Niño and La Niña in southern Africa across the region's summertime wet season, taken here to be November–April (Fig. 2). Our intention is to build a more complete understanding of the controls on daily precipitation and to probe whether the behavior of precipitation between warm and cold ENSO extremes are asymmetric, which has implications for subseasonal forecasts. We examine the variability of daily precipitation characteristics—daily average rainfall, precipitation days (>1 mm), and heavy precipitation days (top quintile)—related to El Niño and La Niña events from 1983 to 2018 for each of the core months of the southern Africa wet season using three estimates of observed precipitation. These estimates are derived from in situ information, remotely sensed data, and a blend of remotely sensed and in situ data. The daily precipitation metrics are examined monthly to determine how the effect of ENSO evolves throughout the rainy season. These metrics—daily average rainfall, precipitation days, and heavy precipitation days—were chosen because of their practical applications. We do not employ models of the Earth system in this study despite a period of record that approaches only 40 years for two reasons: we want to establish an empirical baseline and we do not want results to be biased toward individual model behaviors, since climate models have been shown to struggle in reproducing features of the southern Africa regional climate (Munday and Washington 2018).

We also explore the mechanisms by which precipitation is delivered to southern Africa monthly during El Niño and La Niña events. We do so by probing the moisture budget in an atmospheric reanalysis across the region's summertime rainy season, which allows for an evaluation of how changes in moisture weighted mass divergence, horizontal water vapor transports, and transient eddies conspire to produce changes in precipitation. Such a diagnostic evaluation of the atmospheric moisture budget provides further insights into the drivers of southern Africa weather and climate and how El Niño and La Niña modulates these drivers.

Given the importance of daily rainfall to agriculture and water availability to the region (Jury 2002), an improved predictive understanding determined from this study may guide more effective early warning over countries with high exposure to weather and climate (Conway et al. 2015). An outline of this paper is as follows: In section 2, we describe the tools and methods employed; in section 3, we discuss the results, including average conditions over southern Africa and how El Niño and La Niña events modulate weather and climate over the region; and in section 4, we provide a summary and discuss the implications of the results.

2. Tools and methods

a. *Precipitation data*

We use three estimates of observed daily precipitation: 1) Climate Hazards Group Infrared Precipitation with Stations (CHIRPS), 2) Climate Prediction Center Unified Gauge-Based Analysis of Daily Precipitation (CPC-Unified), and

TABLE 1. List of El Niño and La Niña events based on ONI.

Month	El Niño	La Niña
November	1986, 1987, 1991, 1994, 1997, 2002, 2004, 2006, 2009, 2014, 2015, 2018	1983, 1984, 1988, 1995, 1998, 1999, 2000, 2005, 2007, 2008, 2010, 2011, 2016, 2017
December	1986, 1987, 1991, 1994, 1997, 2002, 2004, 2006, 2009, 2014, 2015, 2018	1983, 1984, 1995, 1998, 1999, 2000, 2005, 2007, 2008, 2010, 2011, 2016, 2017
January	1983, 1987, 1988, 1992, 1995, 1998, 2003, 2005, 2007, 2010, 2015, 2016, 2019	1984, 1985, 1989, 1996, 1999, 2000, 2001, 2006, 2008, 2009, 2011, 2012, 2018
February	1983, 1987, 1988, 1992, 1995, 1998, 2003, 2005, 2010, 2015, 2016, 2019	1985, 1989, 1996, 1999, 2000, 2001, 2006, 2008, 2009, 2011, 2012, 2018
March	1983, 1987, 1992, 1995, 1998, 2010, 2015, 2016, 2019	1985, 1989, 1996, 1999, 2000, 2006, 2008, 2009, 2011, 2012, 2018
April	1982, 1983, 1987, 1992, 1998, 2015, 2016, 2019	1985, 1989, 1999, 2000, 2008, 2011

3) Precipitation Estimation from Remotely Sensed Information using Artificial Neural Networks–Climate Data Record (PERSIANN). We chose these datasets because they are constructed differently, and they are used in the weather, climate, and applications communities.

CHIRPS (Funk et al. 2015), available on a 0.05° × 0.05° fixed latitude–longitude grid, is derived by blending cold cloud duration observations from five infrared satellite products and available station precipitation observations. CHIRPS draws on archives of station observations, including the Global Historical Climate Network, the Global Summary of the Day, the World Meteorological Organization's Global Telecommunication System, the Southern African Science Service Centre for Climate Change and Adaptive Land Management, and precipitation made available by select national and international agencies. Like other precipitation datasets, the density of station observations included in CHIRPS varies in space and time, which makes the blending of satellite data with the station observations a key feature of CHIRPS.

CPC-Unified (Chen et al. 2008), available on a 0.5° × 0.5° fixed latitude–longitude grid, is based on station precipitation observations. CPC-Unified draws on archives of station observations, including Global Historical Climate Network, the Global Summary of the Day, the World Meteorological Organization's Global Telecommunication System, and national and international agencies. CPC-Unified considers orography and implements quality control techniques based on comparisons with satellite-derived precipitation and model forecasts.

PERSIANN (Ashouri et al. 2015), available on a 0.25° × 0.25° fixed latitude–longitude grid, is based on remotely sensed information only. PERSIANN applies a neural network–based algorithm to GridSat-B1 infrared satellite observations and the National Centers for Environmental Prediction stage IV hourly precipitation data. Biases are then removed using the Global Precipitation Climatology Project (Adler et al. 2003) monthly precipitation product.

Results based on the three precipitation datasets are qualitatively similar for their common period of 1983–2018. We present analyses based on CHIRPS in the paper, and results based on PERSIANN and CPC-Unified are provided in the online supplemental material.

b. *Precipitation metrics*

We consider three daily precipitation metrics during each month of southern Africa's austral summer rainy season: daily average precipitation, precipitation days, and heavy precipitation days. These metrics were chosen because of their practical applications. Daily average precipitation is defined as the average daily rainfall during a given month. Precipitation days are defined as the number of days during each month in which precipitation exceeds 1 mm. Heavy rain days are those falling within the upper quintile of the rainfall distribution of wet days based on 1983–2018.

c. *El Niño and La Niña*

We use the NOAA Climate Prediction Center (CPC) catalog of El Niño and La Niña events[1] to examine the association of precipitation characteristics and ENSO. This catalog is based on 3-month overlapping seasons: December–February, January–March, . . . , November–January. El Niño events occur when the Niño-3.4 region (5°N–5°S, 120°–170°W) SST anomaly exceeds 0.5°C for at least five consecutive overlapping 3-month seasons. La Niña events occur when the Niño-3.4 region SST anomaly falls below −0.5°C for at least five consecutive overlapping 3-month seasons. SST are based on the Extended Reconstructed SST dataset version 5 (ERSSTv5; Huang et al. 2017) and anomalies of SST are based on centered 30-yr periods updated every five years.

We temporally disaggregate 3-month seasons from the CPC ENSO event catalog to obtain months that qualify as El Niño and La Niña (Table 1). The disaggregation is based on the center month of the 3-month season. For example, CPC designated the October–December 3-month season in 1997 to be an El Niño period, so we identify November 1997 as El Niño. Similarly, February 2011 is considered La Niña since the 2011 January–March period was determined to be La Niña.

[1] https://origin.cpc.ncep.noaa.gov/products/analysis_monitoring/ensostuff/ONI_v5.php.

d. Moisture budget

We probe the atmospheric moisture budget to gain physical insights that underpin a predictive understanding of daily average precipitation related to El Niño and La Niña during each month of the southern Africa summertime wet season. We employ the method of Seager and Henderson (2013) to arrive at a form of the moisture budget equation that allows us to diagnose the effects of anomalous moisture weighted mass divergence, horizontal water vapor transports, and transient eddies on precipitation changes related to warm and cold ENSO extremes. This evaluation of the moisture budget is based on the ERA5 reanalysis (Hersbach et al. 2020) analyzed at 3-h increments on a 0.25° × 0.25° fixed latitude–longitude grid and 37 pressure levels.

We begin with a common form of the moisture budget equation, shown in Eq. (13) of Seager and Henderson (2013):

$$P = E - \frac{1}{g\rho_w}\frac{\partial}{\partial t}\int_0^{p_s} q\, dp - \frac{1}{g\rho_w}\nabla \cdot \int_0^{p_s} q\mathbf{V}\, dp. \tag{1}$$

Equation (1) states that precipitation P is balanced by evaporation E, the tendency of vertically integrated moisture, and the divergence of vertically integrated moisture flux. In Eq. (1), g is the acceleration due to gravity, ρ_w is the density of water vapor, p is atmospheric pressure, p_s is the surface pressure, q is the specific humidity, and $\mathbf{V}$ is the horizontal wind, comprising zonal u and meridional v components.

Vertical integrals in Eq. (1) are rewritten as pressure weighted sums since we evaluate the ERA5 reanalysis at discrete vertical levels. The summation is over vertical layers k with thickness Δp_k, of which there are $K_{i,j}$, where i, j indicate longitude and latitude, respectively:

$$P \approx E - \frac{1}{g\rho_w}\frac{\partial}{\partial t}\sum_{k=1}^{K_{i,j}} q\,\Delta p_k - \frac{1}{g\rho_w}\nabla \cdot \sum_{k=1}^{K_{i,j}} q_k \mathbf{V}_k\,\Delta p_k. \tag{2}$$

Diagnosing the contributions of mass divergence, water vapor transports, and transient eddies requires that variables in the vertically integrated moisture flux term be separated into means and deviations from the mean. For example, specific humidity at a 3-h increment as in our evaluation of ERA5 can be expressed as

$$q_3 = \overline{q} + q_3' = \overline{\overline{q}} + \widehat{\overline{q}} + q_3', \tag{3}$$

where primes denote a departure of 3-hourly data from a monthly mean, bars denote a monthly average, hats denote monthly average departures from the long-term monthly mean, and double bars denote the long-term monthly mean.

Substituting expansions like Eq. (3) for specific humidity and the horizontal wind vector into the vertically integrated moisture flux term in Eq. (2) and expressing the resulting expression as the monthly precipitation from the long-term mean yields Eq. (33) in Seager and Henderson (2013):

$$\widehat{\overline{P}} \approx \widehat{\overline{E}} - \frac{1}{g\rho_w}\frac{\partial}{\partial t}\sum_{k=1}^{K_{i,j}} q\,\Delta p_k - \frac{1}{g\rho_w}\nabla \cdot \sum_{k=1}^{K_{i,j}} \widehat{\overline{\mathbf{V}}_k\,\overline{q}_k\,\overline{\Delta p}_k} - \frac{1}{g\rho_w}\nabla \cdot \sum_{k=1}^{K_{i,j}} \widehat{\overline{\mathbf{V}_{3,k}' q_{3,k}'}\,\overline{\Delta p}_k}. \tag{4}$$

Note that Seager and Henderson (2013) neglect the vertically integrated moisture tendency term in their Eq. (33) because of its magnitude relative to the other terms. We verify this later for southern Africa related to El Niño and La Niña.

To examine contributions by moisture weighted mass divergence and horizontal water vapor transports, the divergence operator is brought inside second term on the right-hand side of Eq. (4), which introduces a surface term. After applying a vector identity and replacing pressure thickness with climatological values, Eq. (35) in Seager and Henderson (2013), in addition to the vertically integrated moisture tendency term, is obtained:

$$\begin{aligned}\widehat{\overline{P}} \approx \widehat{\overline{E}} &- \frac{1}{g\rho_w}\frac{\partial}{\partial t}\sum_{k=1}^{K_{i,j}} q\,\Delta p_k - \frac{1}{g\rho_w}\sum_{k=1}^{K_{i,j}} \widehat{(\overline{q}_k \nabla \cdot \overline{\mathbf{V}}_k)}\,\overline{\overline{\Delta p}_k} \\ &- \frac{1}{g\rho_w}\sum_{k=1}^{K_{i,j}} \widehat{(\overline{\mathbf{V}}_k \cdot \nabla \overline{q}_k)}\,\overline{\overline{\Delta p}_k} - \frac{1}{g\rho_w}\nabla \cdot \sum_{k=1}^{K_{i,j}} \widehat{(\overline{\mathbf{V}_{3,k}' q_{3,k}'})}\,\overline{\overline{\Delta p}_k} \\ &- \frac{1}{g\rho_w}\widehat{\overline{q_s \mathbf{V}_s \cdot \nabla p_s}}.\end{aligned} \tag{5}$$

For monthly mean anomalies, Eq. (5) states that precipitation is balanced by evaporation, the vertically integrated moisture tendency term, the moisture weighted mass divergence, horizontal water vapor advection, transient eddies based on 3-hourly data, and a surface term. We use Eq. (5) to attribute changes in monthly precipitation characteristics related to El Niño and La Niña to contributions by moisture weighted mass divergence, horizontal water vapor transports, and transient eddies anomalies. We will also show that contributions by anomalous evaporation, the vertically integrated moisture tendency, and the surface term related to warm and cold ENSO extremes are small.

Since deviations from the monthly mean are considered at 3-h increments, the transient term of the moisture budget equation includes variations on time scales as short as three hours. The transient term therefore captures key high-frequency features of southern Africa weather and climate, including but not limited to tropical temperate troughs.

e. Statistical significance

We use a bootstrapping approach to determine if changes in precipitation characteristics or terms of the moisture budget equation during El Niño and La Niña are statistically different at the 5% level from conditions based on a 1983–2018 mean. Random samples corresponding to the number of days that qualify as either El Niño or La Niña are drawn from the entire population. The samples are screened for the precipitation characteristic or term of the moisture budget equation. This process is repeated 10 000 times to build a distribution, which is then used to identify the 2.5% and 97.5% confidence levels corresponding to a two-sided p value of 0.05.

3. Results

a. Mean precipitation characteristics

To establish a baseline from which changes in precipitation characteristics related to El Niño and La Niña can be compared, we begin with a description of spatiotemporal variations in average daily precipitation, precipitation days, and heavy precipitation days for November–April 1983–2018. We

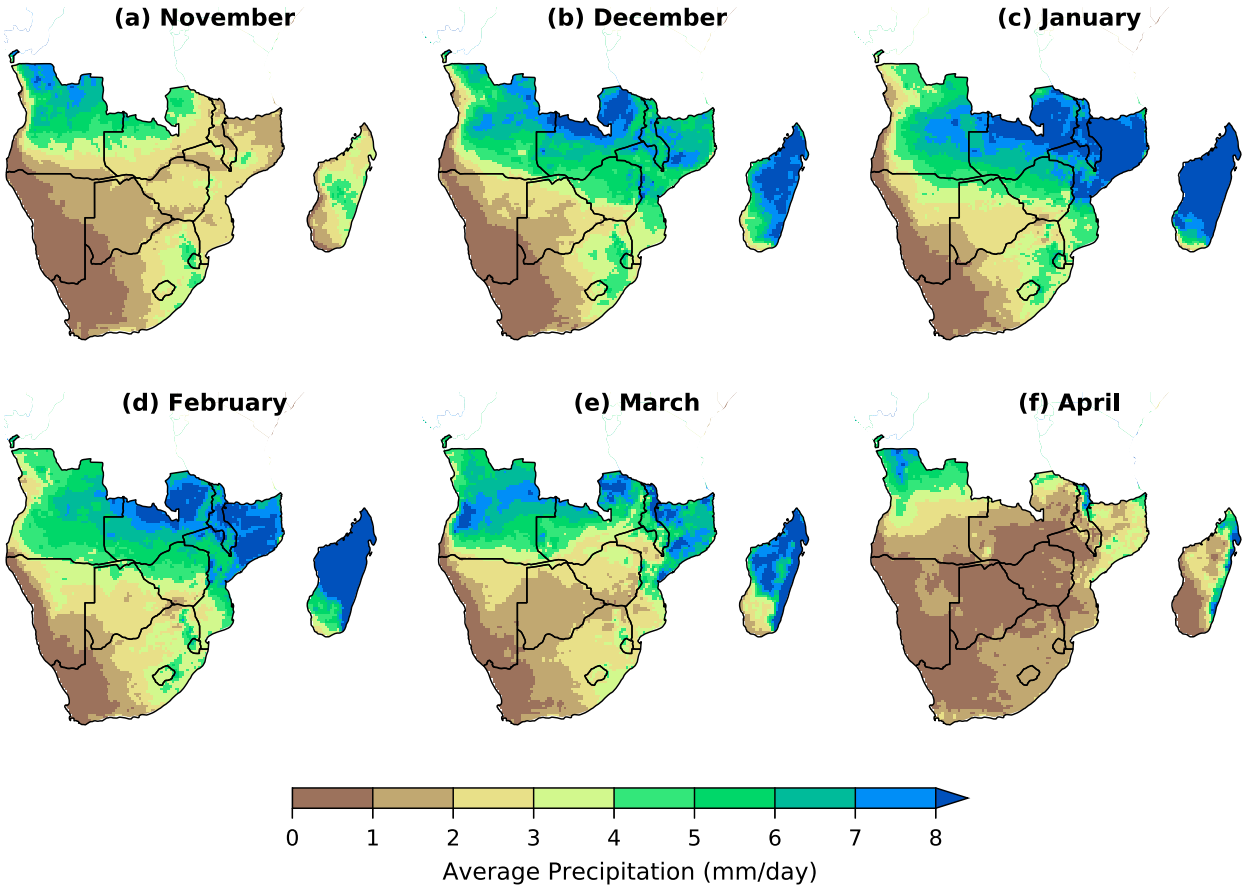

FIG. 3. Average precipitation (mm day^{-1}) based on CHIRPS.

use the entire 36-yr record since the sample size of ENSO neutral is small (Table 1).

Daily average precipitation across southern Africa varies greatly in space and time during austral summer, from meager precipitation over the semiarid steppes over of Namibia, Botswana, and central-western South Africa to abundant precipitation over humid subtropical areas of Zambia, Malawi, and northern Mozambique (Fig. 3; see also Figs. S1 and S2 in the online supplemental material). The seasonal increase in daily average precipitation begins in November as the tropical rain belt dips southward into the region. Also, in November, southeastern South Africa and Swaziland experience a local maximum in precipitation as rain-bearing tropical temperate troughs (TTTs) make their way onshore (e.g., Todd and Washington 1999; Blamey and Reason 2009; Ratna et al. 2013; Macron et al. 2014; Wiston and Mphale 2019). The rainy season winds down in March and ends in April, as the tropical rain belt lifts northward and the occurrence of TTTs become less frequent. Although qualitatively quite similar, differences in average monthly precipitation between CHIRPS, CPC-Unified, and PERSIANN are apparent. CHIRPS and PERSIANN are most similar in terms of magnitude and pattern because they are both based on remotely sensed information, although precipitation from PERSIANN is smoother owing to its coarser resolution. CPC-Unified captures the evolution of the precipitation pattern during southern Africa's rainy season but differs greatly from CHIRPS and PERSIANN in terms of magnitude, likely because it is based on observations that are sparse in space and time.

December–February constitute the height of the southern Africa rainy season, as daily average precipitation reaches its greatest values regionwide (Fig. 3; see also Figs. S1 and S2). The tropical rain belt becomes firmly established in the northern part of southern Africa and TTTs become more frequent over the southern part of the region. Daily average precipitation more than 6 mm day^{-1} related to the tropical rain belt covers a wide swath of the region, including Zambia, Malawi, northern Mozambique, northeastern Zimbabwe, and the majority of Madagascar. Tropical cyclones are also a semicommon occurrence over these areas, particularly for Madagascar and north-central Mozambique (Fitchett and Grab 2014). Coastal areas of southern Mozambique and southeastern South Africa receive precipitation from rain-bearing TTTs, but in amounts that are comparably less than the northern part of the region. Precipitation in central South Africa, Botswana, and eastern Namibia is unique, since this area receives comparably less precipitation (~2 mm day^{-1}), as neither the tropical rain belt nor TTTs affect this area with

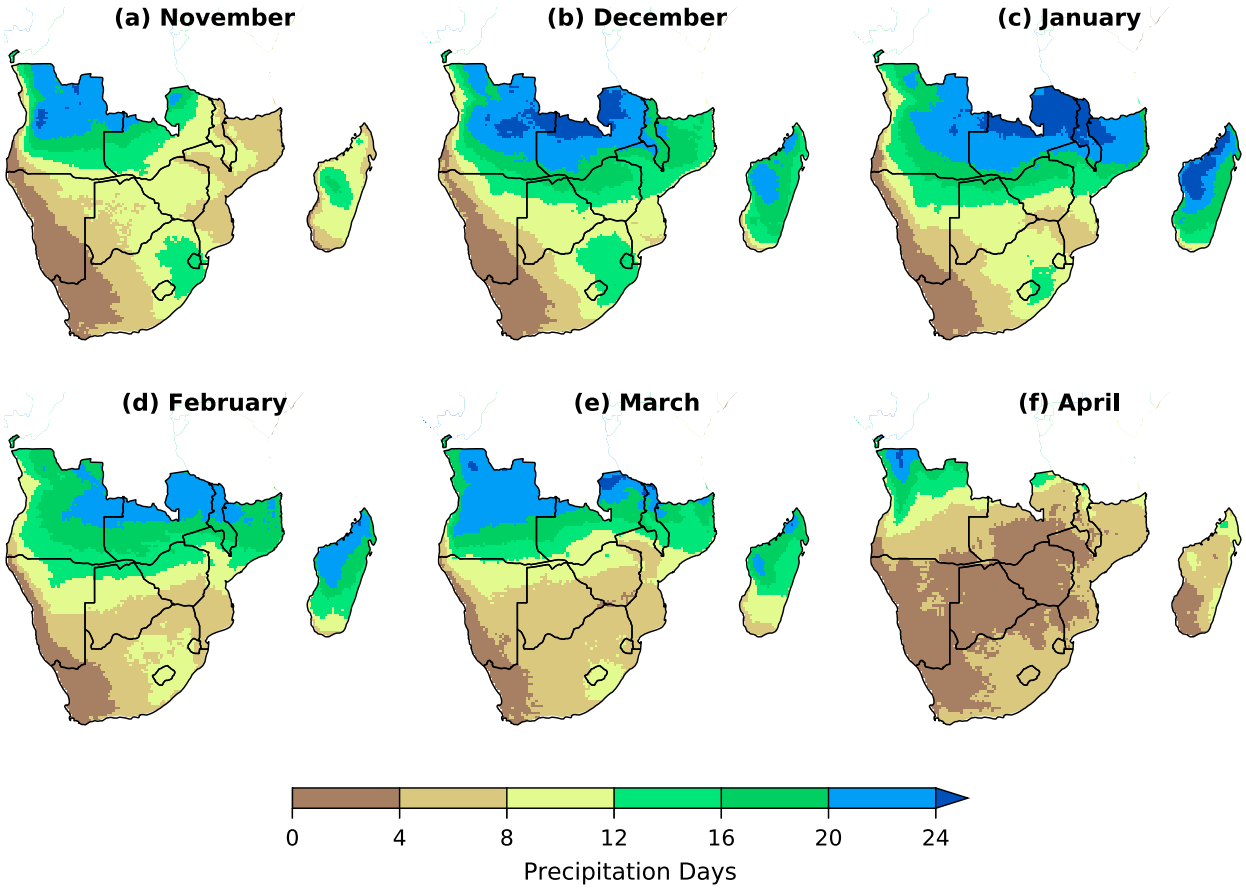

FIG. 4. Average precipitation days (>1 mm) based on CHIRPS.

vigor. While the rainy season begins to wind down in March, appreciable daily precipitation is nonetheless observed in a spatial pattern that resembles December–February. The austral summertime rainy season ends in April, as average daily precipitation of less than 1 mm day^{-1} engulfs the region.

The spatiotemporal variability of precipitation days generally scales with daily average precipitation across the region (Fig. 4; see also Figs. S3 and S4). Precipitation days are most frequent over the subtropical humid areas in the northern part of the region that are directly affected by the tropical rain belt. More than half, and upward of three-quarters, of days in December–February receive precipitation over humid subtropical areas like Zambia, Malawi, and northern Mozambique, with the 3-month maximum occurring in January. Precipitation days are comparably less frequent over the semiarid areas in the southern and western part of the region that receive most of the precipitation from rain bearing TTTs or are only somewhat affected by the tropical rain belt. Subtropical areas including southern Mozambique, northeastern South Africa, Zimbabwe, and Botswana receive the bulk of their precipitation during the core of the rainy season in approximately 8 days per month. While similar in terms of the patterns of precipitation days, it is important to note that the magnitudes differ between CHIRPS and PERSIANN. There are more precipitation days in PERSIANN than CHIRPS regionwide.

Heavy precipitation days demonstrate a distinct preference for occurring in January–March over most of the region (Fig. 5; see also Figs. S5 and S6). This is interesting because the timing is offset by about one month from the seasonal maximum precipitation accumulation, shown in Fig. 3 as occurring in December–February. The likelihood of heavy precipitation days is greatest over the entire region in January. This includes areas like Mozambique, Malawi, Zambia, northern Zimbabwe, and Angola, where at least one and upward of two days per year experience such an event. This likelihood decreases somewhat across the region in February and March but is nonetheless still noteworthy for areas like Zambia in February and central-northern Mozambique in March. Subtropical areas, like southern Mozambique, southern Zimbabwe, and Botswana experience comparably fewer heavy precipitation days by virtue of having fewer precipitation days, but their greatest likelihood for such an event occurs in January and March. The number of heavy precipitation days does not vary as much between CHIRPS and PERSIANN like they do for the number of precipitation days. A possible reason for the difference is that heavy precipitation days are defined relative to the

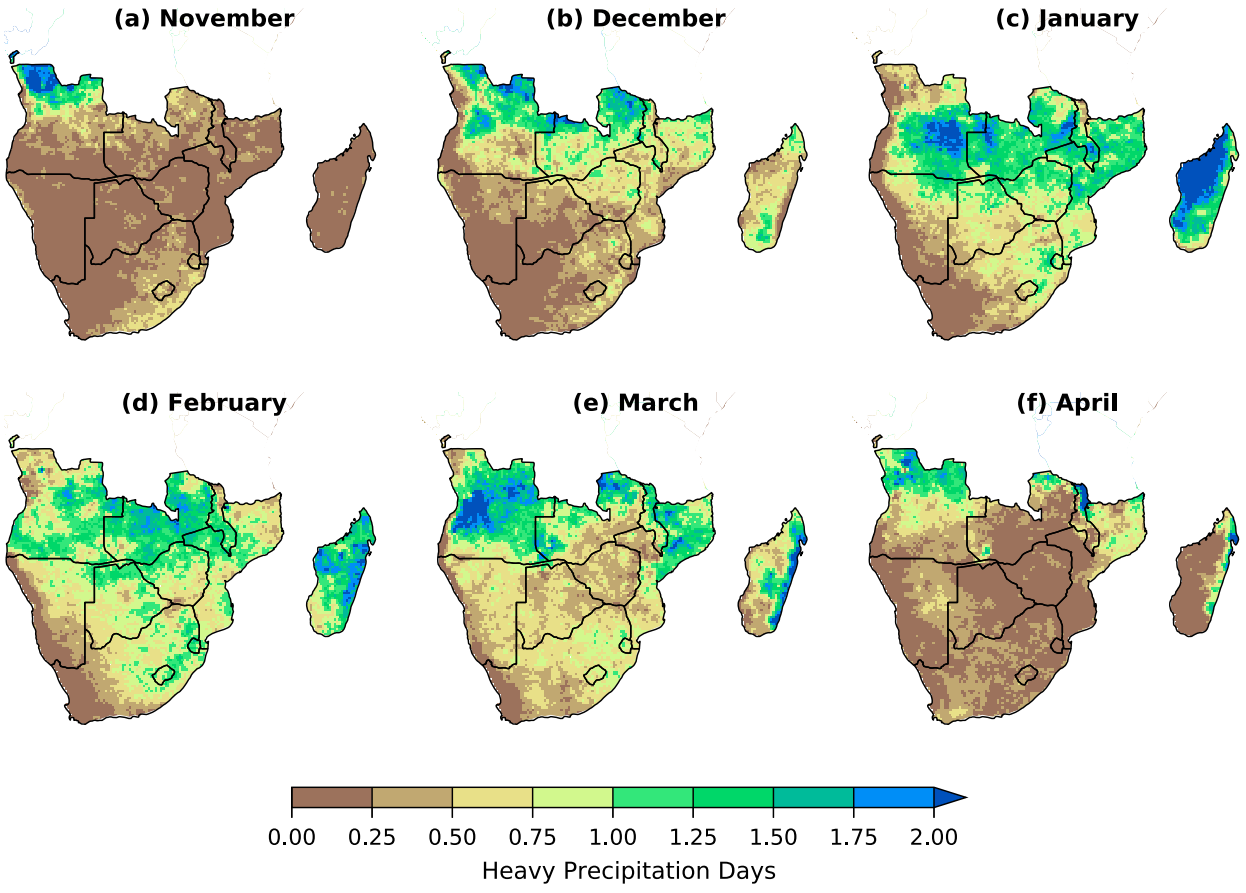

FIG. 5. Average heavy precipitation days (top quintile) based on CHIRPS.

distribution of rainfall in each dataset while precipitation days are defined by the same physical threshold that is applied to all datasets.

b. *Changes in precipitation characteristics related to El Niño and La Niña*

We probe the spatiotemporal variations in monthly precipitation, precipitation days, and heavy precipitation days during each month of the southern Africa wet season related to El Niño and La Niña. Results are expressed as a difference from average conditions shown in Figs. 3–5. We expect that seasonal precipitation anomalies related to El Niño and La Niña (Figs. 1 and 2) occur during months that make up the season. We test these expectations in the following.

El Niño and La Niña are related to statistically significant daily average precipitation anomalies across southern Africa, highlighted by a notable evolution in their spatial pattern throughout the region's summertime rainy season (Fig. 6; see also Figs. S7 and S8). The anomalies are largest during December–March, the core months of the rainy season, yet largely insignificant in November and April, which mark the beginning and end of the rainy season, respectively. The anomalies are most prominent over the transition area between the humid subtropical climates to the north and the semiarid climates to the south, including central-southern Mozambique, Zimbabwe, southwestern Zambia, and Botswana. Results based on CHIRPS, CPC-Unified, and PERSIANN are qualitatively quite similar in terms of patterns and magnitudes, although significant precipitation anomalies are noticeably more widespread from PERSIANN, particularly in February and March.

During December–February, the magnitude of daily precipitation anomalies related to El Niño builds from one month to the next, culminating in a large area of significantly below average precipitation over the central part of the region (left column in Figs. 6, S7, and S8). This large area, which covers an east-to-west oriented band across central and southern Mozambique, Zimbabwe, Botswana, southwestern Zambia, southeastern Angola, and northeastern Namibia, is especially pronounced in January and February. El Niño is not related to below average precipitation over the wettest areas of the region, like northern Mozambique and northeastern Zambia, during the core of the rainy season. During March, daily precipitation anomalies related to El Niño are generally mild, with a small area of below average precipitation covering southern Angola, and northern Namibia.

Daily precipitation anomalies related to La Niña do not exhibit the same seasonal evolution as El Niño (right column in Figs. 6, S7, and S8). In December, significant above average precipitation anomalies span central Mozambique, Zimbabwe,

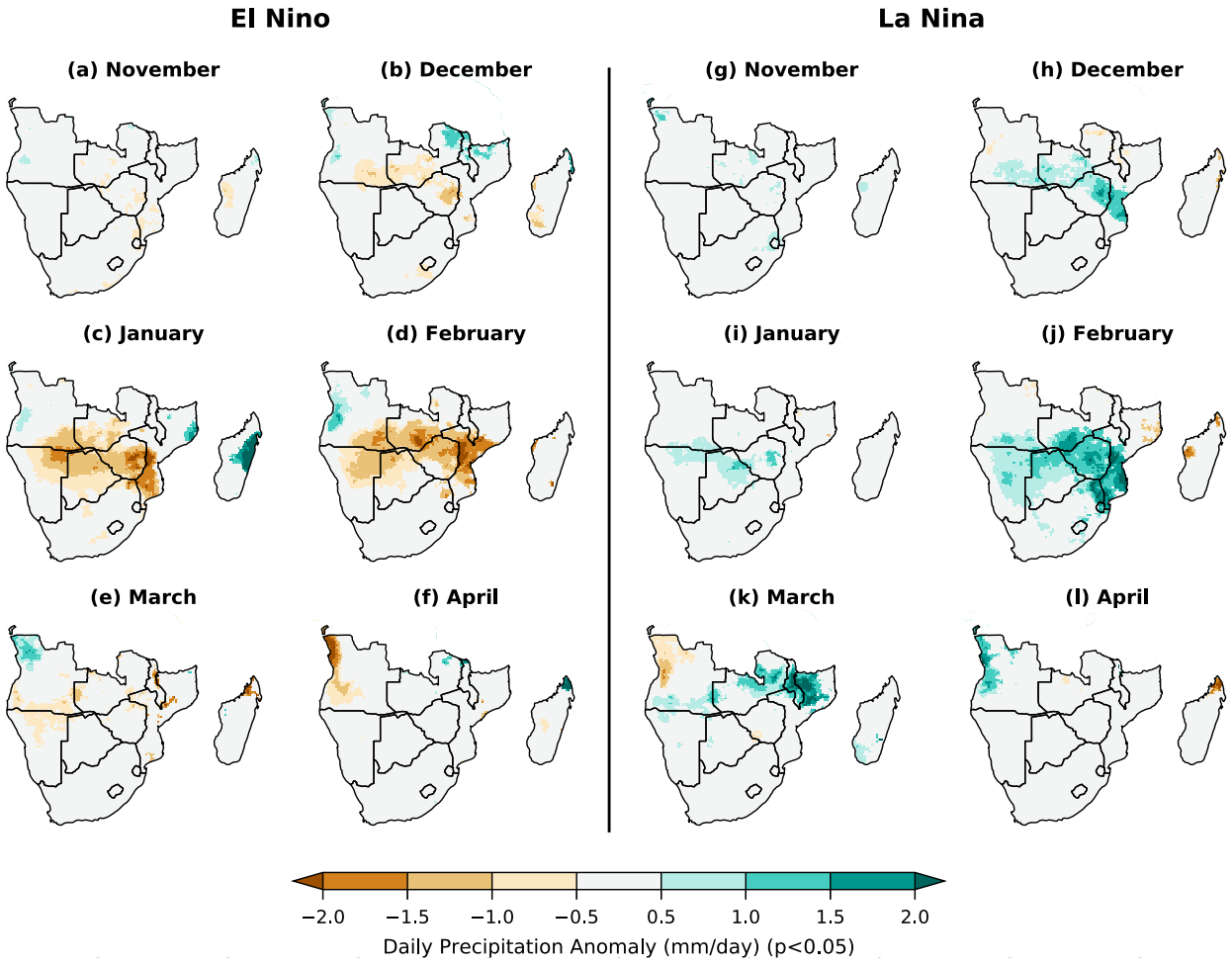

FIG. 6. Precipitation anomaly (mm day^{-1}) related to El Niño and La Niña based on CHIRPS. Shaded values are significant at $p < 0.05$.

southwestern Zambia, and southeastern Angola. Despite being squarely in the core of the rainy season, precipitation anomalies related to La Niña in January are weak, as the spatial extent of statistically significantly above average precipitation anomalies is limited to the intersection of Angola and Namibia, Botswana, and parts of Zimbabwe. In February, the spatial extent of statistically significant above average precipitation anomalies is widespread and covers almost the entirety of the region south of 20° south latitude, except southeastern Botswana and central South Africa. In March, the spatial extent of statistically significant above average precipitation anomalies is again limited, but primarily over northern Mozambique and northeastern Zambia.

An asymmetry in the southern African precipitation response to opposite ENSO extremes is suggested by dissimilarities in the patterns and absolute magnitudes of below average precipitation related to El Niño and above average precipitation related to La Niña. This is especially evident in January, as El Niño is related to widespread below average precipitation across much of semiarid southern Africa, including Mozambique, Botswana, Zimbabwe, and Namibia, while La Niña is related to weak and isolated areas of above average precipitation in Zimbabwe, Botswana, Angola, and Namibia (Figs. 6, S7, and S8). We test for the existence of such an asymmetry across the region's summertime wet season by probing symmetric and asymmetric precipitation components, taken to be the precipitation difference between El Niño and La Niña and the precipitation summation of El Niño and La Niña, respectively (Figs. 7, S9, and S10), as in Hoerling et al. (1997).

The magnitude of the symmetric component of southern Africa precipitation related to El Niño and La Niña is greater than the asymmetric component during all months, suggesting that the summertime precipitation response to ENSO over the region is largely linear (Figs. 7, S9, and S10). The pattern of the symmetric precipitation component is dominated by an east-to-west oriented band across central and southern Mozambique, Zimbabwe, Botswana, southwestern Zambia, southeastern Angola, and northeastern Namibia during December–February. The symmetric component is also prominent in March over northern parts of the region, including Mozambique, Zambia, and Angola. Nonetheless, the magnitude of the asymmetric component is

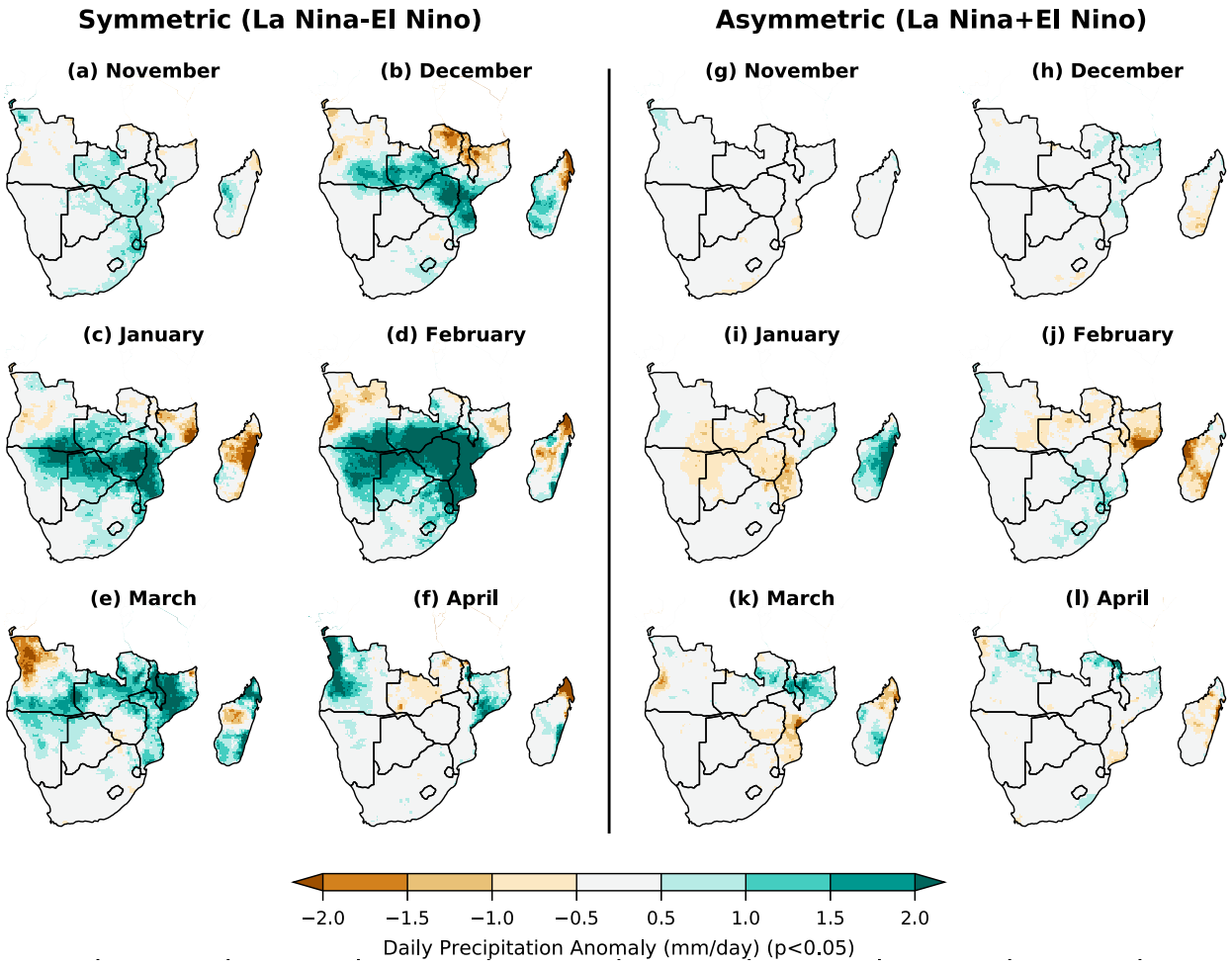

FIG. 7. Symmetric component of ENSO-related precipitation anomalies based on the difference between La Niña and El Niño and the asymmetric component of ENSO-related precipitation anomalies based on the sum of La Niña and El Niño. Precipitation is based on CHIRPS (mm day^{-1}). Shaded values are significant at $p < 0.05$.

statistically significant over a large part of the region during January–March, which suggests that a noteworthy nonlinearity may exist in the ENSO-related precipitation response over southern Africa. The pattern of the asymmetric precipitation component related to ENSO is generally weak, yet widespread across southern Africa in January and February, and confined to Mozambique and Malawi in March.

The robustness of an asymmetric component to the evolution of precipitation anomalies related to ENSO extremes across the southern Africa summertime wet season may have implications for subseasonal forecasts. The existence of an asymmetry suggests that precipitation forecasts based on ENSO should not assume that daily precipitation anomalies between El Niño and La Niña are equal and opposite. It is important to note, however, that these results are based on an empirical sample that spans just four decades (Table 1), and further research will be needed to probe this possible asymmetry. The asymmetry would need to be confirmed using analyses based on empirical data that span a longer time period and established in simulations from reliable climate models.

El Niño and La Niña are also related to statistically significant precipitation day anomalies across southern Africa (Figs. 8, S11, and S12). These monthly patterns resemble (Figs. 6, S7, and S8) and are correlated with (Table 2) the daily average precipitation anomalies during many months of the rainy season. PERSIANN indicates larger precipitation day anomalies related to El Niño and La Niña than CHIRPS or CPC-Unified because it indicates more precipitation days on average (Figs. 3, S3, and S4). Precipitation day anomalies are most prominent over the transition area between the humid subtropical climate to the north and the semiarid climates to the south and west. This zonally oriented band across central southern Africa spanning central-southern Mozambique, Zimbabwe, southwestern Zambia, and Botswana experiences approximately 8–12 days in which at least 1 mm of precipitation is observed during the core of the rainy season (Figs. 4, S3, and S4). La Niña (El Niño) increases (decreases) the number of such days by up to 3 over these areas, constituting a 20%–30% change in precipitation days relative to average. Like the daily average precipitation anomaly, El Niño is related to a significant

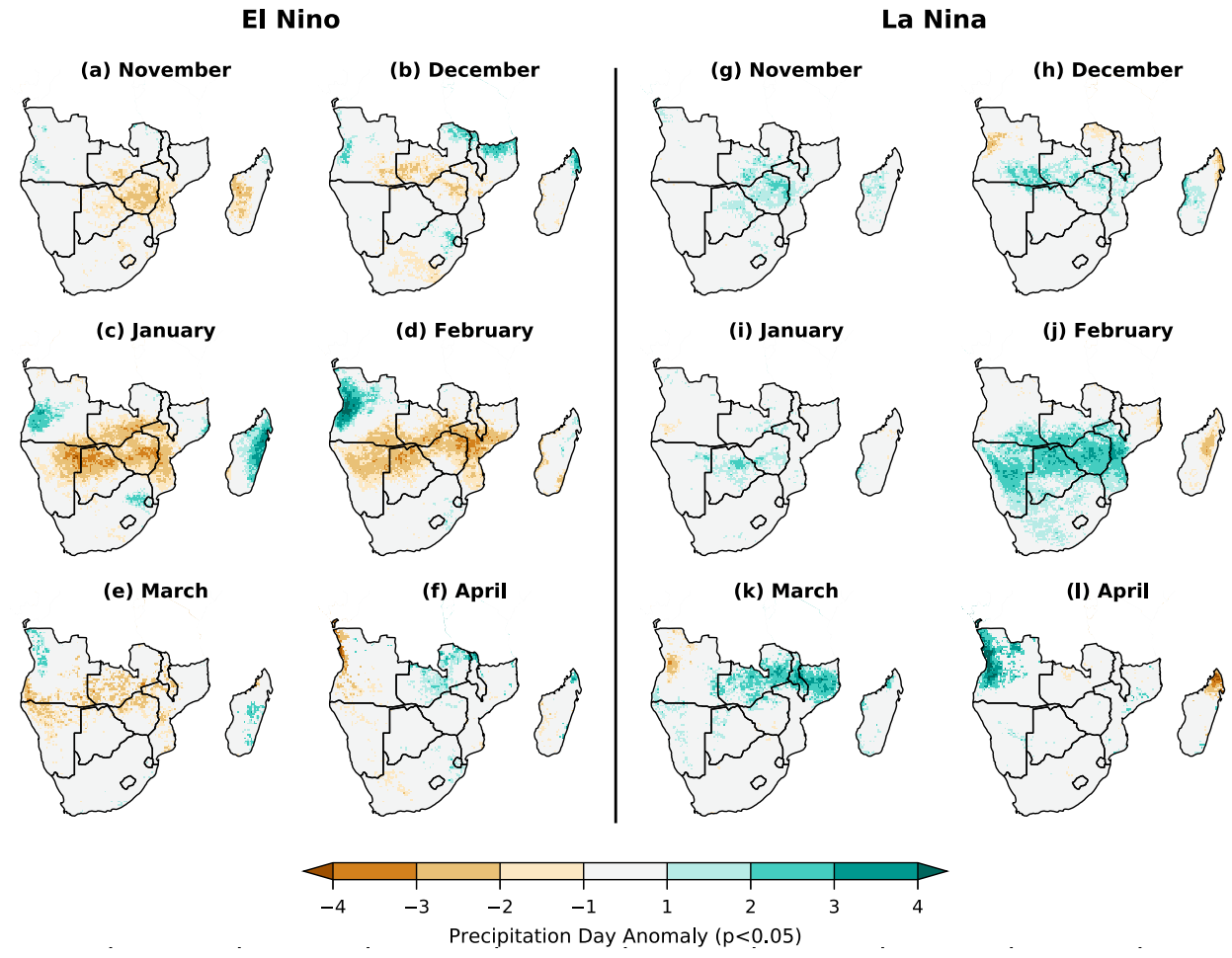

FIG. 8. Precipitation day (>1 mm) anomaly related to El Niño and La Niña based on CHIRPS. Shaded values are significant at $p < 0.05$.

decrease in the number of rain days, principally during January and February. La Niña is related to significant increases in the number of rain days during February over nearly all southern Africa and over Zambia and northern Mozambique during March.

The changes in precipitation days related to El Niño and La Niña have implications for how we interpret rainfall regimes over southern Africa. First, the similarities between the patterns of monthly precipitation day anomalies (Figs. 8, S11, and S12) and average daily precipitation anomalies (Figs. 6, S7, and S8) suggest that ENSO's effect on daily average precipitation is at least partly due to how often it rains. This is key over semiarid southern Africa, including central-southern Mozambique, Zimbabwe, Botswana, and southwestern Zambia, because some of these areas only experience around 8 precipitation days per month during the height of the rainy season, and fewer opportunities for precipitation will have consequences. Beyond altering the daily average precipitation for a given month, changes in the number of precipitation days related to El Niño and La Niña will alter the likelihood of prolonged dry spells. For example, a 30% reduction in the number of precipitation days during El Niño for an area that on average experiences 8 such days per month will increase the likelihood of long dry spells.

Likewise, the monthly patterns of heavy precipitation day anomalies related to El Niño and La Niña (Figs. 9, S13, and S14) resemble the patterns of precipitation day anomalies (Figs. 8, S11, and S12). That is, heavy precipitation days exhibit significant deviations from average during the height of the rainy

TABLE 2. Pattern correlation between monthly precipitation and precipitation day anomalies related to El Niño and La Niña based on CHIRPS over the domain 35°–15°S, 10°–42°E.

ENSO phase	November	December	January	February	March	April
El Niño	0.75	0.82	0.78	0.83	0.61	0.65
La Niña	0.66	0.75	0.48	0.78	0.81	0.61

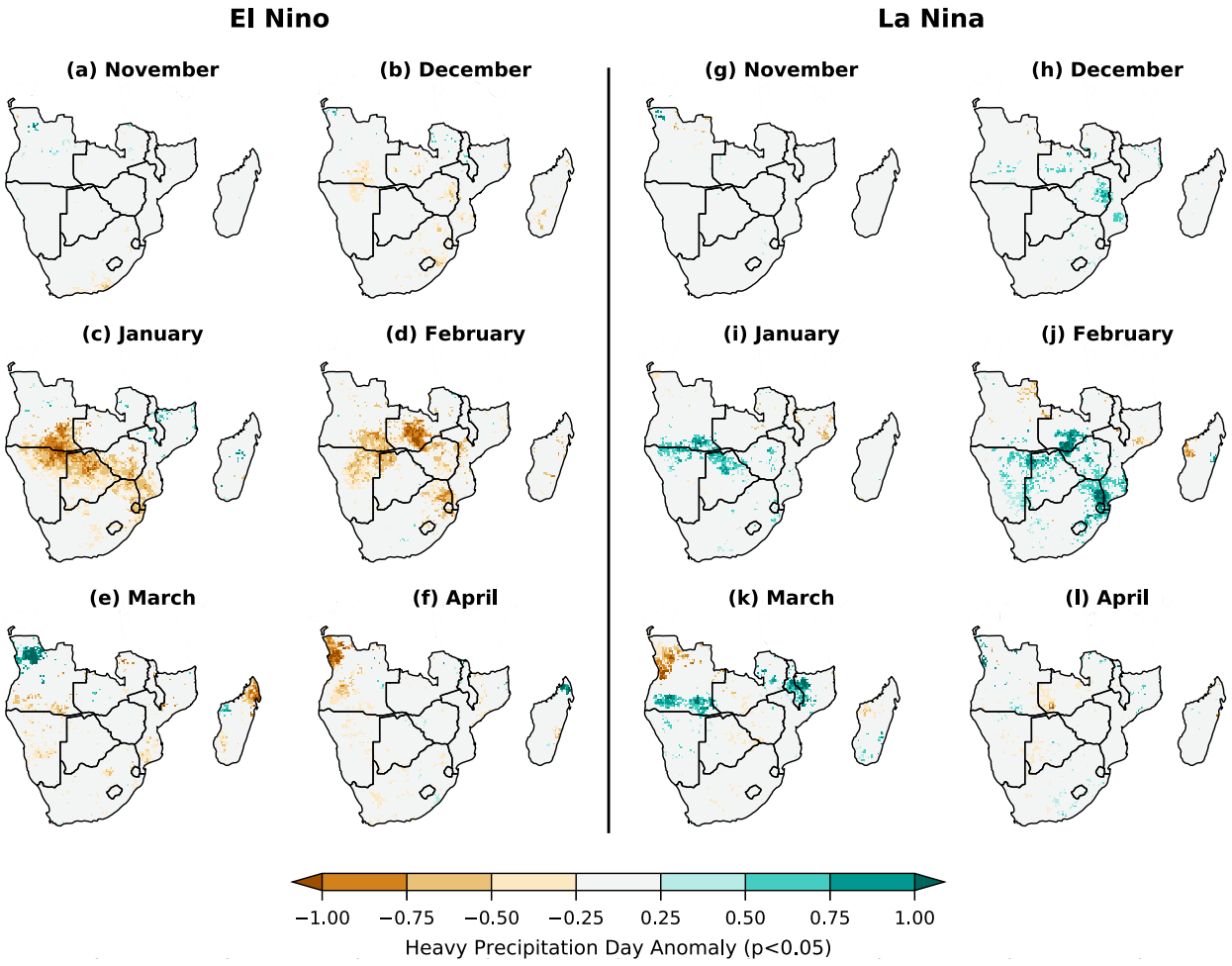

FIG. 9. Heavy precipitation (top quintile) day anomaly related to El Niño and La Niña based on CHIRPS. Shaded values are significant at $p < 0.05$.

season, January, and February during El Niño and February for La Niña. This makes sense because increases in precipitation days increase the opportunity for heavy precipitation. It is important to note, however, that while there is some coherence in the pattern of heavy precipitation days, the patterns are somewhat scattered because heavy precipitation tends to be localized and the top quintile of precipitation is difficult to achieve.

c. *Mean moisture budget*

Toward better understanding the mechanisms by which precipitation is delivered to southern Africa and to establish a baseline from which to physically diagnose ENSO-related precipitation anomalies, we begin with an analysis of the mean atmospheric moisture budget over southern Africa [Eq. (2)], shown in terms of evaporation minus vertically integrated moisture flux divergence (Fig. 10). This formulation of the moisture budget equation also allows us to compare mean monthly precipitation in the ERA5 reanalysis with observed estimates (Figs. 3, S1, and S2) to qualitatively judge the fidelity of the reanalysis in representing key features of southern Africa weather and climate. A visual comparison between ERA5 and CHIRPS monthly average precipitation indicates a rather strong agreement between the two and supports our use of this reanalysis in diagnosing southern Africa weather and climate. The ERA5 representation of southern Africa precipitation indicates a marked improvement (Zhang et al. 2013) over its predecessor, ERA-Interim (Dee et al. 2011).

The movement of prominent features in the large-scale atmospheric circulation over Africa and the southern Indian Ocean are key to maintaining the atmospheric moisture budget, and therefore the progression of the tropical rain belt during southern Africa's austral summer rainy season. In November, the rain belt is noticeable over Angola and the Democratic Republic of the Congo and moves southward in December and February related to the seasonal progression and intensification of the Angola low (e.g., Howard and Washington 2018), which is apparent in the behavior of the vertically integrated moisture flux (streamlines in Fig. 10). Also contributing to the southward movement and intensification of the rain belt in the eastern part of the region is development of the Mozambique Channel trough in January and February

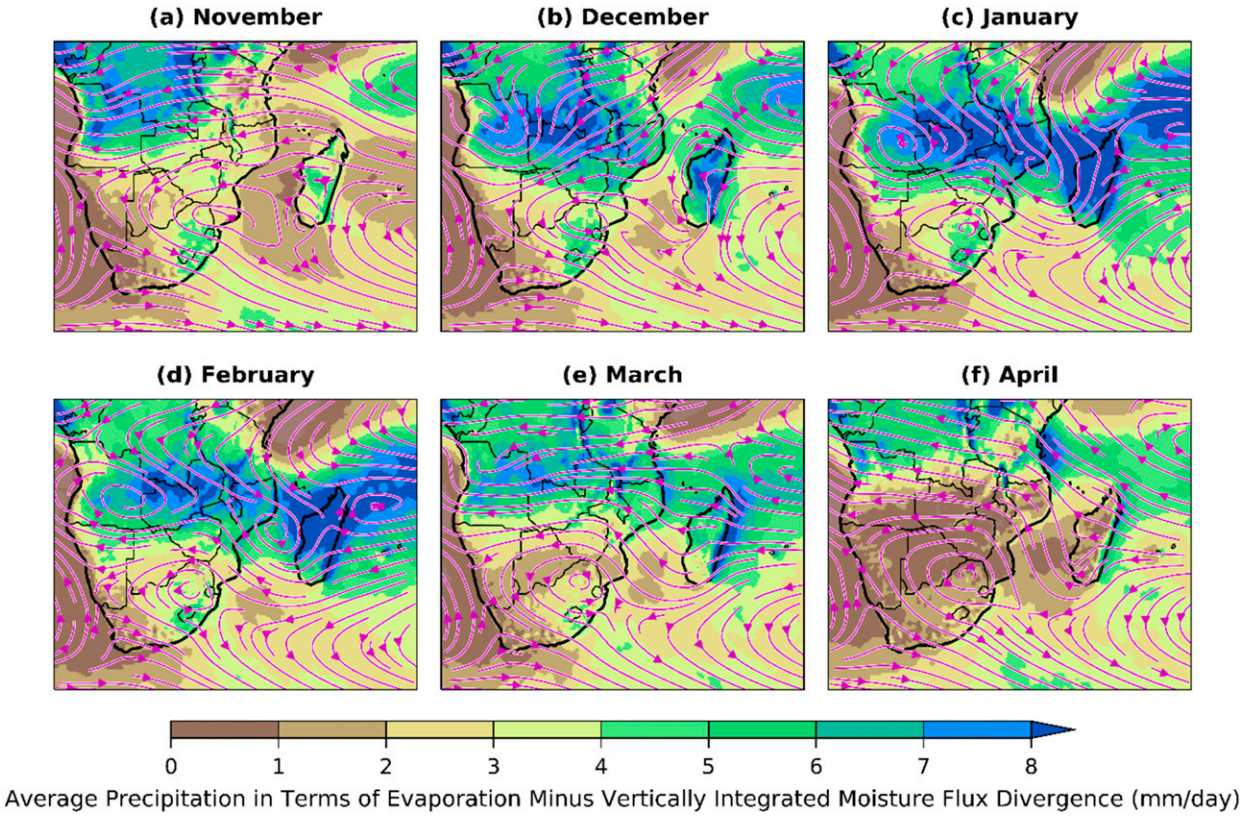

FIG. 10. Average precipitation in terms of evaporation minus vertically integrated moisture flux divergence (shading; mm day^{-1}) and vertically integrated moisture flux (streamlines).

(Lazenby et al. 2016; Barimalala et al. 2020), which is also visible in the vertically integrated moisture flux field. The tropical rain belt reaches its southernmost extent in February and lifts northward in March and April as the Mozambique Channel trough weakens and the Angola low both weakens and moves northward.

While an in-depth discussion on tropical rain belts is beyond the focus of this paper, it is nonetheless important to point out that arguments have been made in the literature as to how the tropical rain belt over central and southern Africa should be characterized. Cook (2000) argued that this rain belt is distinct from the intertropical convergence zone (ITCZ) and should be labeled the South Indian convergence zone (SICZ). Similarly, Nicholson (2018) argued that the ITCZ is not an appropriate paradigm in which to characterize the rain belt over central and southern Africa and advocated for further research on the topic.

d. *Changes in moisture budget related to El Niño and La Niña*

Vertically integrated moisture flux divergence anomalies related to El Niño (Fig. 11) and La Niña (Fig. 12) mirror the spatial patterns and evolution of daily average precipitation anomalies (Fig. 6) during the southern Africa summertime rainy season. This suggests, and we confirm, that contributions to moisture budget anomalies by changes in evaporation (Figs. S15 and S16), the vertically integrated moisture tendency term (Figs. S17 and S18), and the surface term (Figs. S19 and S20) from Eq. (5) related to warm and cold ENSO extremes are small. This reinforces the importance of the vertically integrated moisture flux divergence term in the moisture budget equation over southern Africa and motivates a diagnosis of how changes in the moisture weighted mass divergence, horizontal moisture transports, and transient eddies lead to precipitation anomalies during each month of the region's austral summer rainy season.

The most prominent feature in the vertically integrated moisture flux over southern Africa related to ENSO is that of anomalous anticyclonic and cyclonic circulation during El Niño and La Niña, respectively (streamlines in Figs. 11 and 12). These anomalous circulation centers encompass almost the entirety of southern Africa and demonstrate a notable evolution throughout the rainy season, consistent with that of the vertically integrated moisture flux divergence (shading in Figs. 11 and 12) and the spatial pattern of daily average precipitation anomalies (Fig. 6).

The subseasonal evolution of anomalous vertically integrated moisture flux and their divergence related to El Niño (Fig. 11) and La Niña (Fig. 12) explain the differences in anomalous precipitation characteristics between warm and cold ENSO events (Fig. 6) during the summertime wet season. El Niño is related to a single anomalous anticyclone in the vertically integrated moisture flux field that is centered over

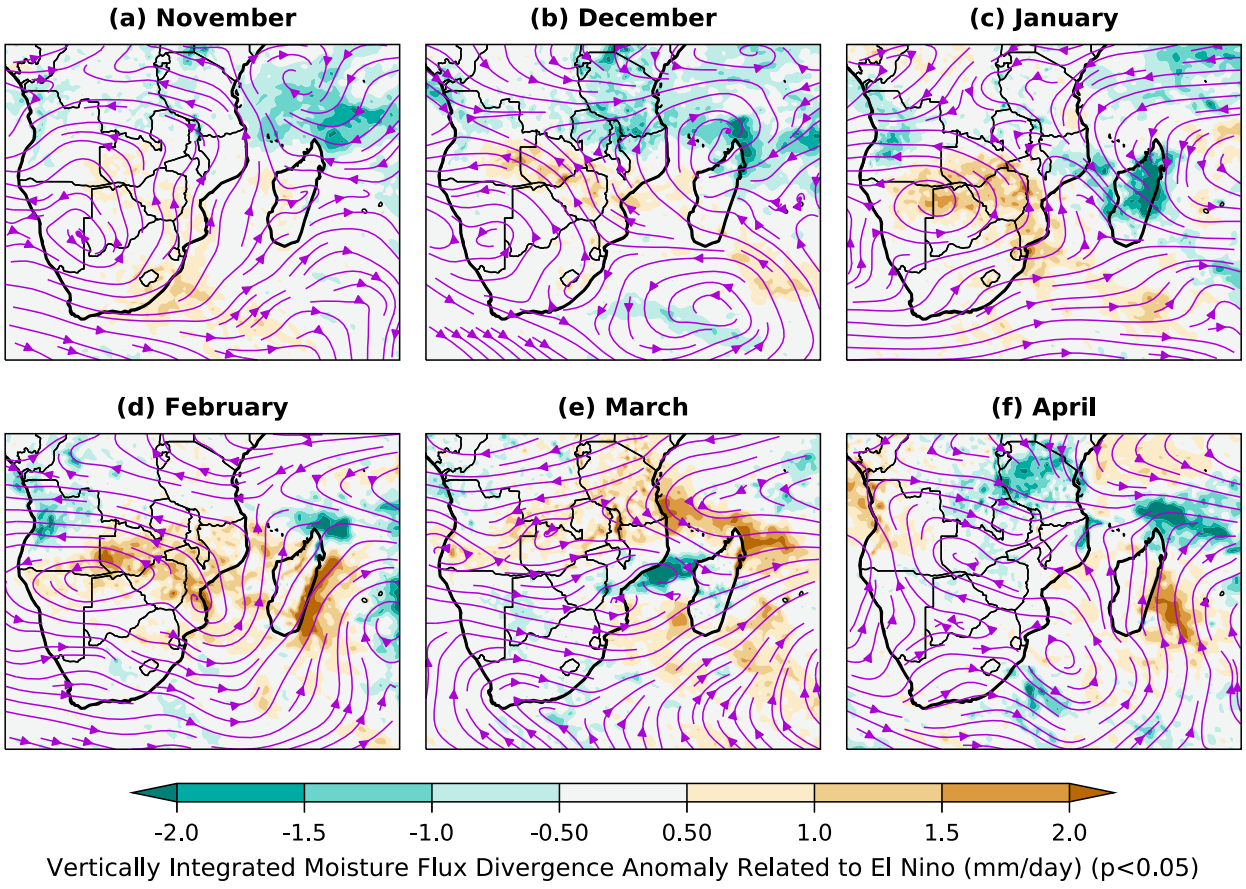

FIG. 11. Vertically integrated moisture flux anomaly (streamlines) and its divergence (shading; mm day^{-1}) related to El Niño. Shaded values are significant at $p < 0.05$.

the intersection of Angola, Namibia, and Botswana, whose effect is to produce widespread and coherent anomalous moisture flux divergence anomalies across much of southern Africa. By contrast, La Niña is related to two diffuse anomalous cyclones in the vertically integrated moisture flux field, one centered over Angola, Namibia, and Botswana and the other centered over the Mozambique Channel, which leads to comparably weak anomalous moisture flux divergence across southern Africa, particularly during December, January, and March. During February, a single cyclonic circulation in the vertically integrated moisture flux field is related to La Niña, resulting in strong moisture flux convergence and therefore increases in precipitation relative to average.

The contributions of moisture weighted mass divergence, horizontal moisture advection, and transient eddies to the vertically integrated moisture flux divergence anomalies associated with El Niño and La Niña are diagnosed to better understand ENSO's physical links to southern Africa precipitation. This diagnosis provides further insights into the mechanisms that drive southern Africa precipitation since the vertically integrated moisture flux divergence term itself cannot distinguish between contributions by moisture weighted mass divergence (i.e., the diffluence and divergence of circulation), moisture advection (i.e., the movement of air across the humidity gradient), or transient eddies (i.e., tropical temperate troughs).

For the core months of southern Africa's austral summer rainy season, December–February, the contribution by the moisture weighted mass divergence term dwarfs the contribution by the moisture advection and transient eddy terms to the total vertically integrated moisture flux divergence anomaly related to both El Niño (Fig. 13) and La Niña (Fig. 14). Note that we only show the core months of the rainy season for brevity, but the same applies for November, March, and April, which experience comparatively weaker anomalous precipitation (Fig. 6). These results indicate that vertical motions due to mass balance considerations are key to southern Africa precipitation related to ENSO, not the movement of air across the humidity gradients in the subcontinent, or fast fluctuations in weather. These results are consistent with Cook (2000), who found that mass divergence dominates the moisture advection contribution to vertically integrated moisture flux divergence over land in an idealized model simulation, and Seager and Naik (2012), who also identified the primacy of the mass divergence contribution to vertically integrated moisture flux divergence related to El Niño and La Niña. These results are also consistent with Hoell and Eischeid

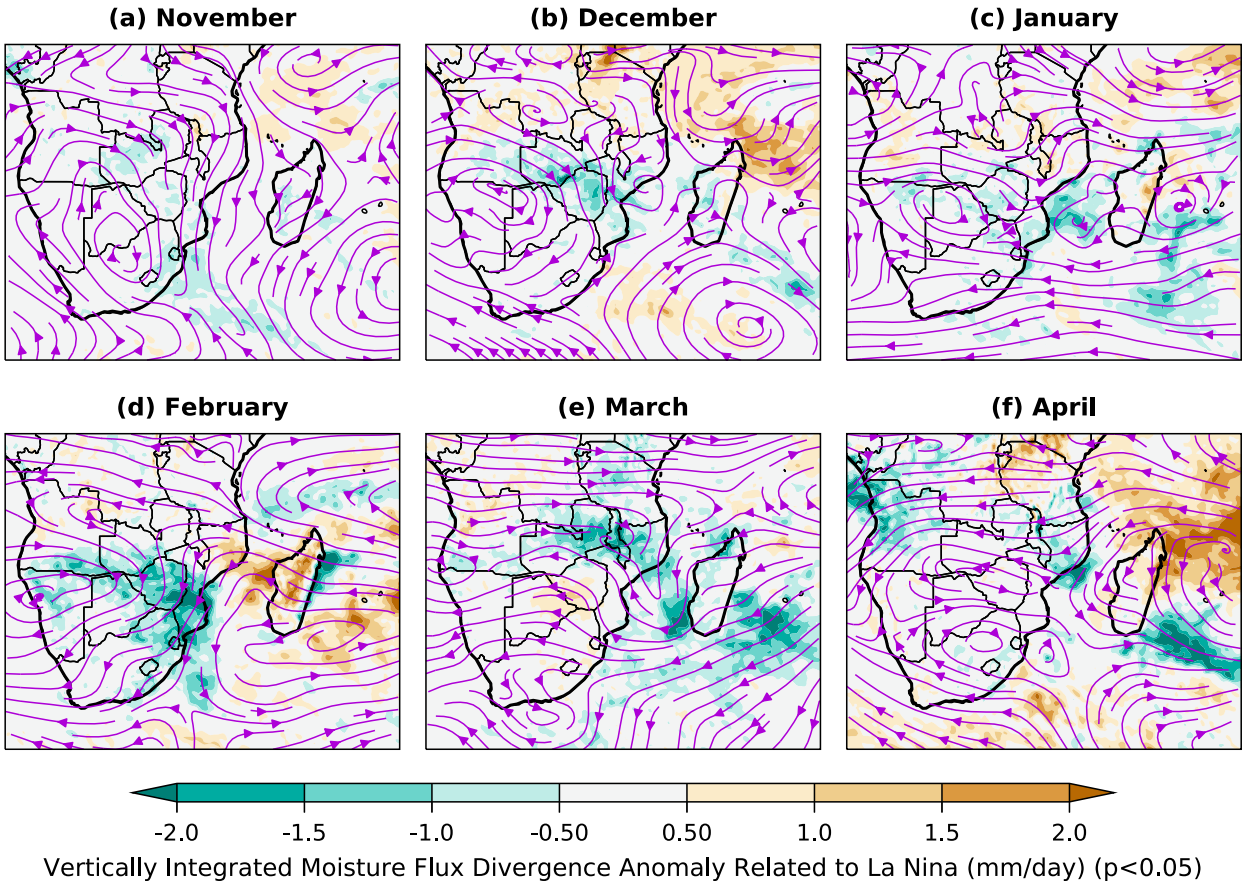

FIG. 12. Vertically integrated moisture flux anomaly (streamlines) and its divergence (shading; mm day^{-1}) related to La Niña. Shaded values are significant at $p < 0.05$.

(2019), who found a close correspondence between vertical motions and precipitation anomalies over southern Africa during ENSO events.

4. Summary and discussion

We examined daily southern Africa precipitation characteristics related to El Niño and La Niña, and the mechanisms by which precipitation is delivered, during each month of the region's rainy season that spans November–April. Using three independently constructed estimates of observed rainfall for 1983–2018, we investigated the spatiotemporal variation of daily average precipitation, precipitation days, and heavy precipitation days related to warm and cold ENSO events. We then examined the atmospheric moisture budget in a widely used atmospheric reanalysis to diagnose how El Niño and La Niña modulate the circulation, moisture weighted mass divergence, water vapor transports, and transient eddies, thereby leading to changes in southern Africa precipitation.

Changes in the atmospheric circulation, and therefore the atmospheric moisture budget, related to El Niño promote an environment that is conducive for widespread decreases in daily average precipitation (Fig. 6) and precipitation days (Fig. 7) during December–February, the core of the southern African rainy season. The magnitude of daily average precipitation and precipitation day anomalies related to El Niño build during this 3-month span, culminating in significantly below average values over an east-to-west oriented band across the transition area between the humid subtropical climate to the north and the semiarid climates to the south and west. This band spans central and southern Mozambique, Zimbabwe, Botswana, southwestern Zambia, southeastern Angola, and northeastern Namibia, with much of that region home to rural, rainfed smallholder agriculture juxtaposed within conservation lands next to wildlife protected areas (Hanks 2003; Makate et al. 2017). Interestingly, El Niño is not related to significant anomalies in precipitation characteristics over the wettest part of the region, which includes northern Mozambique and northeastern Zambia, during any month of the rainy season. The statistically significant anomalous precipitation characteristics over southern Africa related to El Niño are driven by anomalous vertically integrated moisture flux divergence during the core of the rainy season (Fig. 11). The vertically integrated moisture flux divergence is caused by a large area of anomalous anticyclonic circulation in the vertically integrated moisture flux due to a weakened Angola low and Mozambique

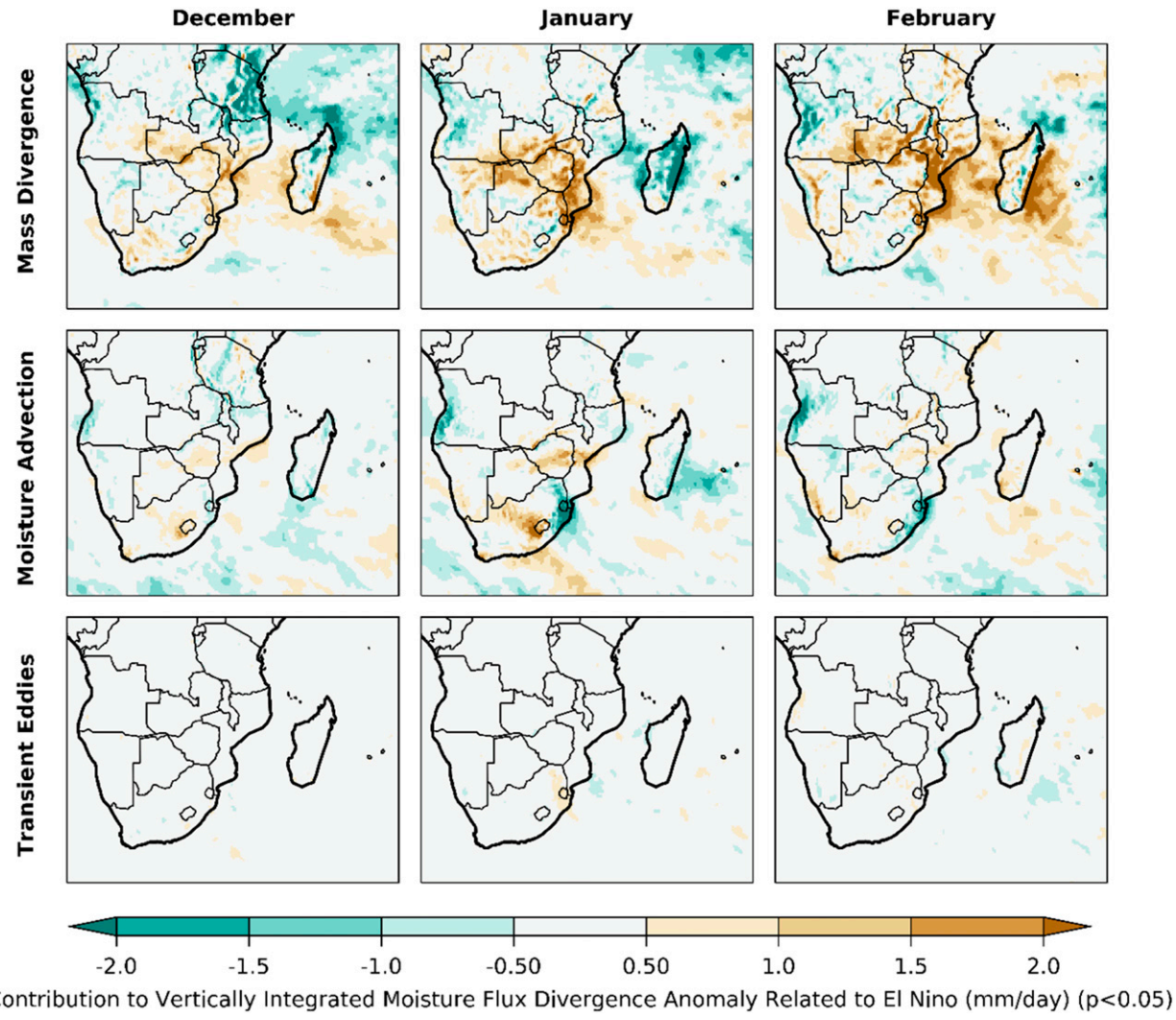

FIG. 13. Contribution to vertically integrated moisture flux divergence anomaly (mm day^{-1}) by (top) moisture weighted mass divergence, (middle) moisture advection, and (bottom) transient eddies related to El Niño. Shaded values are significant at $p < 0.05$.

Channel trough. By separating the vertically integrated moisture flux divergence into parts related to mass divergence, advection, and transients, we find that mass divergence is the primary contributor to vertically integrated moisture flux and therefore precipitation anomalies related to El Niño (Fig. 13).

Changes in the atmospheric circulation related to La Niña promote an environment that is conducive for widespread increases in daily average precipitation (Fig. 6) and precipitation days (Fig. 7) over southern Africa. The statistically significant anomalies, however, do not exhibit the same evolution across the rainy season as during El Niño. Significant anomalies in daily average precipitation and precipitation days related to La Niña span central Mozambique, Zimbabwe, southwestern Zambia, and southeastern Angola in December. However, in January, these statistically significant anomalies are weak and limited to the intersection of Angola and Namibia, Botswana, and parts of Zimbabwe even though this is the height of the rainy season region wide. Another reversal is found in February, as widespread significant precipitation anomalies related to La Niña are observed, covering nearly the entire region south of 20°S latitude. During March, significant increases in daily precipitation and precipitation day anomalies over northern Mozambique and eastern Zambia are related to La Niña. The month-to-month variability in precipitation characteristics can be explained by variations in the anomalous cyclonic circulation in the vertically integrated moisture flux field over southern Africa. Strong and significant precipitation anomalies during February are related to a single coherent cyclonic circulation in the vertically integrated moisture flux field, leading to a concentrated are vertically integrated convergence (Fig. 12). By contrast, during December and January, two anomalous cyclones prevail—one over Botswana and the other over the Mozambique Channel—which leads to comparably weak anomalous moisture flux divergence across southern Africa.

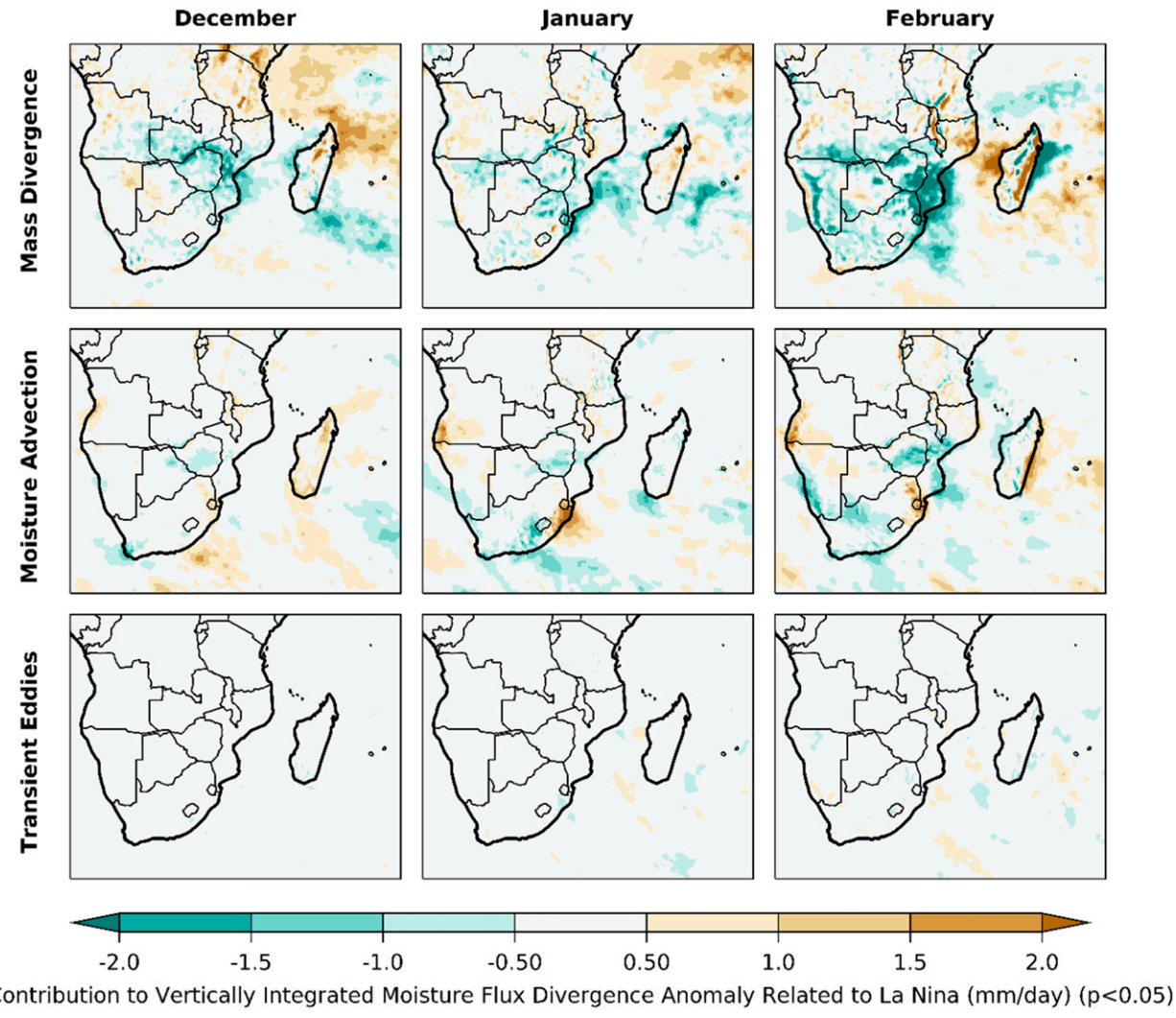

FIG. 14. Contribution to vertically integrated moisture flux divergence anomaly (mm day^{-1}) by (top) moisture weighted mass divergence, (middle) moisture advection, and (bottom) transient eddies related to La Niña. Shaded values are significant at $p < 0.05$.

Like El Niño, mass divergence is the primary contributor to vertically integrated moisture flux divergence and precipitation anomalies related to La Niña (Fig. 14).

Dissimilarities in the patterns and absolute magnitudes of below average precipitation related to El Niño and above average precipitation related to La Niña suggest an asymmetry in the southern African precipitation response to opposite ENSO extremes (Fig. 7). We probed this asymmetry and found that the summertime precipitation response to ENSO over the region is largely linear. However, a nonlinear component is nonetheless statistically significant over a large part of southern Africa during January–March, which overlaps the core of the region's rainy season. The implications for sustainable food production are critical as timing and consistency in rainfall will directly impact crop yield production (Ray et al. 2015).

With that underlying consideration, the existence of an asymmetry would suggest that precipitation forecasts based on ENSO should not assume that daily precipitation anomalies between El Niño and La Niña are equal and opposite. Given the empirical sample spanning just four decades upon which this analysis is based, this asymmetry will need to be confirmed using analyses based on empirical data that span a longer time period and established in simulations from reliable climate models. As noted previously, Earth system models were not employed in this study because we wanted to establish an empirical baseline and we did not want results to be biased toward individual model architectures, particularly those run at coarse resolutions that may poorly simulate daily precipitation (e.g., Wehner et al. 2014).

A primary motivation for this study was to build a more complete understanding of the controls of daily southern Africa precipitation across the region's austral summer rainy season. The relevance for this motivation is that the spatiotemporal variability of precipitation across the southern Africa rainy season has direct implications for rural Africa communities, especially those that practice smallholder agriculture as their

main source of subsistence (e.g., Gelcer et al. 2018) and toward the development of policy initiatives for monitoring and measuring progress toward sustainable development goals in the critical agricultural sector of southern Africa. The potential for El Niño to create a drier season in which dry spells become more common due to decreases in rain days, and La Niña to do the opposite, will impact agriculture yields, which are sensitive to soil moisture changes during germination and reproductive growth stages of crops. Such ENSO-related changes in food production will impact acute and chronic food insecurity with the potential to increase uncertainty in the timing and type of decisions made related to agricultural practices (e.g., Kotir 2011; Cairns et al. 2013). While previous studies relating ENSO and southern Africa climate have largely focused on seasonal and annual behaviors, this study denotes a better characterization of southern Africa's weather and climate on subseasonal time scales, charting new territory and potentially providing an improved predictive understanding to guide effective early warning. The principal findings of this are of importance to subseasonal forecasts that guide agriculture, water, and power sectors in countries with high exposure to weather and climate.

Acknowledgments. We gratefully acknowledge the support of the Famine Early Warning Systems Network, and Marty Hoerling and three anonymous reviewers, whose comments led to an improved analysis and presentation.

REFERENCES

Adler, R. F., and Coauthors, 2003: The version-2 Global Precipitation Climatology Project (GPCP) monthly precipitation analysis (1979–present). *J. Hydrometeor.*, **4**, 1147–1167, https://doi.org/10.1175/1525-7541(2003)004<1147:TVGPCP>2.0.CO;2.

Ashouri, H., and Coauthors, 2015: PERSIANN-CDR: Daily precipitation climate data record from multisatellite observations for hydrological and climate studies. *Bull. Amer. Meteor. Soc.*, **96**, 69–83, https://doi.org/10.1175/BAMS-D-13-00068.1.

Barimalala, R., R. C. Blamey, F. Desbiolles, and C. J. C. Reason, 2020: Variability in the Mozambique Channel trough and impacts on southeast African rainfall. *J. Climate*, **33**, 749–765, https://doi.org/10.1175/JCLI-D-19-0267.1.

Behera, S. K., and T. Yamagata, 2001: Subtropical SST dipole events in the southern Indian Ocean. *Geophys. Res. Lett.*, **28**, 327–330, https://doi.org/10.1029/2000GL011451.

Blamey, R. C., and C. J. C. Reason, 2009: Numerical simulation of a mesoscale convective system over the east coast of South Africa. *Tellus*, **61A**, 17–34, https://doi.org/10.1111/j.1600-0870.2008.00366.x.

——, S. R. Kolusu, P. Mahlalela, M. C. Todd, and C. J. C. Reason, 2018: The role of regional circulation features in regulating El Niño climate impacts over southern Africa: A comparison of the 2015/2016 drought with previous events. *Int. J. Climatol.*, **38**, 4276–4295, https://doi.org/10.1002/joc.5668.

Cairns, J. E., J. Hellin, K. Sonder, J. L. Araus, J. F. MacRobert, C. Thierfelder, and B. M. Prasanna, 2013: Adapting maize production to climate change in sub-Saharan Africa. *Food Secur.*, **5**, 345–360, https://doi.org/10.1007/s12571-013-0256-x.

Capotondi, A., and Coauthors, 2015: Understanding ENSO diversity. *Bull. Amer. Meteor. Soc.*, **96**, 921–938, https://doi.org/10.1175/BAMS-D-13-00117.1.

Chen, M., W. Shi, P. Xie, V. B. S. Silva, V. E. Kousky, R. W. Higgins, and J. E. Janowiak, 2008: Assessing objective techniques for gauge-based analyses of global daily precipitation. *J. Geophys. Res.*, **113**, D04110, https://doi.org/10.1029/2007JD009132.

Conway, D., and Coauthors, 2015: Climate and southern Africa's water–energy–food nexus. *Nat. Climate Change*, **5**, 837–846, https://doi.org/10.1038/nclimate2735.

Cook, K. H., 2000: The South Indian convergence zone and interannual rainfall variability over southern Africa. *J. Climate*, **13**, 3789–3804, https://doi.org/10.1175/1520-0442(2000)013<3789:TSICZA>2.0.CO;2.

——, 2001: A Southern Hemisphere wave response to ENSO with implications for southern Africa precipitation. *J. Atmos. Sci.*, **58**, 2146–2162, https://doi.org/10.1175/1520-0469(2001)058<2146:ASHWRT>2.0.CO;2.

Crétat, J., B. Pohl, B. Dieppois, S. Berthou, and J. Pergaud, 2019: The Angola low: Relationship with southern African rainfall and ENSO. *Climate Dyn.*, **52**, 1783–1803, https://doi.org/10.1007/s00382-018-4222-3.

Dee, D. P., and Coauthors, 2011: The ERA-Interim reanalysis: Configuration and performance of the data assimilation system. *Quart. J. Roy. Meteor. Soc.*, **137**, 553–597, https://doi.org/10.1002/qj.828.

Dixon, J., A. Gulliver, and D. Gibbon, 2001: *Farming Systems and Poverty: Improving Farmers' Livelihoods in a Changing World*. FAO and World Bank, 407 pp.

Fitchett, J. M., and S. W. Grab, 2014: A 66-year tropical cyclone record for south-east Africa: Temporal trends in a global context. *Int. J. Climatol.*, **34**, 3604–3615, https://doi.org/10.1002/joc.3932.

Funk, C., and Coauthors, 2015: The Climate Hazards Infrared Precipitation with Stations—A new environmental record for monitoring extremes. *Sci. Data*, **2**, 150066, https://doi.org/10.1038/sdata.2015.66.

Gaughan, A. E., C. G. Staub, A. Hoell, A. Weaver, and P. R. Waylen, 2016: Inter- and intra-annual precipitation variability and associated relationships to ENSO and the IOD in southern Africa. *Int. J. Climatol.*, **36**, 1643–1656, https://doi.org/10.1002/joc.4448.

Gelcer, E., and Coauthors, 2018: Influence of El Niño–Southern Oscillation (ENSO) on agroclimatic zoning for tomato in Mozambique. *Agric. For. Meteor.*, **248**, 316–328, https://doi.org/10.1016/j.agrformet.2017.10.002.

Gore, M., B. J. Abiodun, and F. Kucharski, 2020: Understanding the influence of ENSO patterns on drought over southern Africa using SPEEDY. *Climate Dyn.*, **54**, 307–327, https://doi.org/10.1007/s00382-019-05002-w.

Hanks, J., 2003: Transfrontier Conservation Areas (TFCAs) in southern Africa. *J. Sustain. For.*, **17**, 127–148, https://doi.org/10.1300/J091v17n01_08.

Hastenrath, S., L. Greischar, and J. van Heerden, 1995: Prediction of the summer rainfall over South Africa. *J. Climate*, **8**, 1511–1518, https://doi.org/10.1175/1520-0442(1995)008<1511:POTSRO>2.0.CO;2.

Hersbach, H., and Coauthors, 2020: The ERA5 global reanalysis. *Quart. J. Roy. Meteor. Soc.*, **146**, 1999–2049, https://doi.org/10.1002/qj.3803.

Hoell, A., and L. Cheng, 2018: Austral summer southern Africa precipitation extremes forced by the El Niño–Southern Oscillation and the subtropical Indian Ocean dipole. *Climate Dyn.*, **50**, 3219–3236, https://doi.org/10.1007/s00382-017-3801-z.

——, and J. Eischeid, 2019: On the interpretation of seasonal southern Africa precipitation prediction skill estimates during

austral summer. *Climate Dyn.*, **53**, 6769–6783, https://doi.org/10.1007/s00382-019-04960-5.

——, C. Funk, T. Magadzire, J. Zinke, and G. Husak, 2015: El Niño–Southern Oscillation diversity and southern Africa teleconnections during austral summer. *Climate Dyn.*, **45**, 1583–1599, https://doi.org/10.1007/s00382-014-2414-z.

——, ——, J. Zinke, and L. Harrison, 2017a: Modulation of the Southern Africa precipitation response to the El Niño Southern Oscillation by the subtropical Indian Ocean dipole. *Climate Dyn.*, **48**, 2529–2540, https://doi.org/10.1007/s00382-016-3220-6.

——, A. E. Gaughan, S. Shukla, and T. Magadzire, 2017b: The hydrologic effects of synchronous El Niño–Southern Oscillation and subtropical Indian Ocean dipole events over southern Africa. *J. Hydrometeor.*, **18**, 2407–2424, https://doi.org/10.1175/JHM-D-16-0294.1.

Hoerling, M. P., A. Kumar, and M. Zhong, 1997: El Niño, La Niña, and the nonlinearity of their teleconnections. *J. Climate*, **10**, 1769–1786, https://doi.org/10.1175/1520-0442(1997)010<1769:ENOLNA>2.0.CO;2.

Howard, E., and R. Washington, 2018: Characterizing the synoptic expression of the Angola low. *J. Climate*, **31**, 7147–7165, https://doi.org/10.1175/JCLI-D-18-0017.1.

Huang, B., and Coauthors, 2017: Extended Reconstructed Sea Surface Temperature, version 5 (ERSSTv5): Upgrades, validations, and intercomparisons. *J. Climate*, **30**, 8179–8205, https://doi.org/10.1175/JCLI-D-16-0836.1.

Hulme, M., 1996: *Climate Change in Southern Africa: An Exploration of Some Potential Impacts and Implications for the SADC Region*. WWF Publication, 104 pp.

Jury, M. R., 2002: Economic impacts of climate variability in South Africa and development of resource prediction models. *J. Appl. Meteor.*, **41**, 46–55, https://doi.org/10.1175/1520-0450(2002)041<0046:EIOCVI>2.0.CO;2.

——, C. McQueen, and K. Levey, 1994: SOI and QBO signals in the African region. *Theor. Appl. Climatol.*, **50**, 103–115, https://doi.org/10.1007/BF00864907.

Kotir, J. H., 2011: Climate change and variability in sub-Saharan Africa: A review of current and future trends and impacts on agriculture and food security. *Environ. Dev. Sustain.*, **13**, 587–605, https://doi.org/10.1007/s10668-010-9278-0.

Lazenby, M. J., M. C. Todd, and Y. Wang, 2016: Climate model simulation of the South Indian Ocean convergence zone: Mean state and variability. *Climate Res.*, **68**, 59–71, https://doi.org/10.3354/cr01382.

Lindesay, C. J., 1990: *Economic and Socio-Political Impacts of Rainfall Variations*. University of Witwatersrand, 181 pp.

Lindesay, J. A., 1988: South African rainfall, the Southern Oscillation and a Southern Hemisphere semi-annual cycle. *J. Climatol.*, **8**, 17–30, https://doi.org/10.1002/joc.3370080103.

Lyon, B., and S. J. Mason, 2007: The 1997–98 summer rainfall season in southern Africa. Part I: Observations. *J. Climate*, **20**, 5134–5148, https://doi.org/10.1175/JCLI4225.1.

——, and ——, 2009: The 1997/98 summer rainfall season in southern Africa. Part II: Model simulations and coupled model forecasts. *J. Climate*, **22**, 3802–3818, https://doi.org/10.1175/2009JCLI2600.1.

Macron, C., B. Pohl, Y. Richard, and M. Bessafi, 2014: How do tropical temperate troughs form and develop over southern Africa? *J. Climate*, **27**, 1633–1647, https://doi.org/10.1175/JCLI-D-13-00175.1.

Makate, C., M. Makate, and N. Mango, 2017: Sustainable agriculture practices and livelihoods in pro-poor smallholder farming systems in southern Africa. *Afr. J. Sci. Technol. Innov. Dev.*, **9**, 269–279, https://doi.org/10.1080/20421338.2017.1322350.

Manatsa, D., C. H. Matarira, and G. Mukwada, 2011: Relative impacts of ENSO and Indian Ocean dipole/zonal mode on east SADC rainfall. *Int. J. Climatol.*, **31**, 558–577, https://doi.org/10.1002/joc.2086.

——, C. J. C. Reason, and G. Mukwada, 2012: On the decoupling of the IODZM from southern Africa summer rainfall variability. *Int. J. Climatol.*, **32**, 727–746, https://doi.org/10.1002/joc.2306.

Marchant, R., C. Mumbi, S. Behera, and T. Yamagata, 2007: The Indian Ocean dipole—The unsung driver of climatic variability in East Africa. *Afr. J. Ecol.*, **45**, 4–16, https://doi.org/10.1111/j.1365-2028.2006.00707.x.

Misra, V., 2003: The influence of Pacific SST variability on the precipitation over southern Africa. *J. Climate*, **16**, 2408–2418, https://doi.org/10.1175/2785.1.

Muboko, N., 2017: The role of transfrontier conservation areas and their institutional framework in natural resource-based conflict management: A review. *J. Sustain. For.*, **36**, 583–603, https://doi.org/10.1080/10549811.2017.1320224.

Munday, C., and R. Washington, 2017: Circulation controls on southern African precipitation in coupled models: The role of the Angola low. *J. Geophys. Res. Atmos.*, **122**, 861–877, https://doi.org/10.1002/2016JD025736.

——, and ——, 2018: Systematic climate model rainfall biases over southern Africa: Links to moisture circulation and topography. *J. Climate*, **31**, 7533–7548, https://doi.org/10.1175/JCLI-D-18-0008.1.

Nhemachena, C., G. Matchaya, C. R. Nhemachena, S. Karuaihe, B. Muchara, and S. Nhlengethwa, 2018: Measuring baseline agriculture-related Sustainable Development Goals Index for southern Africa. *Sustainability*, **10**, 849, https://doi.org/10.3390/su10030849.

Niang, I., O. C. Ruppel, M. A. Abdrabo, A. Essel, C. Lennard, J. Padgham, and P. Urquhart, 2014: Africa. *Climate Change 2014: Impacts, Adaptation, and Vulnerability*. V. R. Barros et al., Eds., Cambridge University Press, 1199–1265.

Nicholson, S. E., 2018: The ITCZ and the seasonal cycle over equatorial Africa. *Bull. Amer. Meteor. Soc.*, **99**, 337–348, https://doi.org/10.1175/BAMS-D-16-0287.1.

——, and D. Entekhabi, 1986: The quasi-periodic behavior of rainfall variability in Africa and its relationship to the Southern Oscillation. *Arch. Meteor. Geophys. Bioclimatol.*, **34A**, 311–348, https://doi.org/10.1007/BF02257765.

——, and J. Kim, 1997: The relationship of the El Niño–Southern Oscillation to African rainfall. *Int. J. Climatol.*, **17**, 117–135, https://doi.org/10.1002/(SICI)1097-0088(199702)17:2<117::AID-JOC84>3.0.CO;2-O.

Pascale, S., B. Pohl, S. B. Kapnick, and H. Zhang, 2019: On the Angola low interannual variability and its role in modulating ENSO effects in southern Africa. *J. Climate*, **32**, 4783–4803, https://doi.org/10.1175/JCLI-D-18-0745.1.

Pomposi, C., C. Funk, S. Shukla, L. Harrison, and T. Magadzire, 2018: Distinguishing southern Africa precipitation response by strength of El Niño events and implications for decision-making. *Environ. Res. Lett.*, **13**, 074015, https://doi.org/10.1088/1748-9326/aacc4c.

Ratna, S. B., S. Behera, J. V. Ratnam, K. Takahashi, and T. Yamagata, 2013: An index for tropical temperate troughs over southern Africa. *Climate Dyn.*, **41**, 421–441, https://doi.org/10.1007/s00382-012-1540-8.

Ratnam, J. V., S. K. Behera, Y. Masumoto, and T. Yamagata, 2014: Remote effects of El Niño and Modoki events on the austral

summer precipitation of southern Africa. *J. Climate*, **27**, 3802–3815, https://doi.org/10.1175/JCLI-D-13-00431.1.

Ray, D., J. Gerber, G. MacDonald, and P. West, 2015: Climate variation explains a third of global crop yield variability. *Nat. Commun.*, **6**, 5989, https://doi.org/10.1038/ncomms6989.

Reason, C. J. C., 2001: Subtropical Indian Ocean SST dipole events and southern African rainfall. *Geophys. Res. Lett.*, **28**, 2225–2227, https://doi.org/10.1029/2000GL012735.

——, and D. Jagadheesha, 2005: A model investigation of recent ENSO impacts over southern Africa. *Meteor. Atmos. Phys.*, **89**, 181–205, https://doi.org/10.1007/s00703-005-0128-9.

——, R. J. Allan, J. A. Lindesay, and T. J. Ansell, 2000: ENSO and climatic signals across the Indian Ocean basin in the global context: Part I, interannual composite patterns. *Int. J. Climatol.*, **20**, 1285–1327, https://doi.org/10.1002/1097-0088(200009)20:11<1285::AID-JOC536>3.0.CO;2-R.

Rocha, A., and I. A. N. Simmonds, 1997: Interannual variability of south-eastern African summer rainfall. Part I: Relationships with air–sea interaction processes. *Int. J. Climatol.*, **17**, 235–265, https://doi.org/10.1002/(SICI)1097-0088(19970315)17:3<235::AID-JOC123>3.0.CO;2-N.

Ropelewski, C. F., and M. S. Halpert, 1987: Global and regional scale precipitation patterns associated with the El Niño/Southern Oscillation. *Mon. Wea. Rev.*, **115**, 1606–1626, https://doi.org/10.1175/1520-0493(1987)115<1606:GARSPP>2.0.CO;2.

Saji, N. H., B. N. Goswami, P. N. Vinayachandran, and T. Yamagata, 1999: A dipole mode in the tropical Indian Ocean. *Nature*, **401**, 360–363, https://doi.org/10.1038/43854.

Seager, R., and N. Naik, 2012: A mechanisms-based approach to detecting recent anthropogenic hydroclimate change. *J. Climate*, **25**, 236–261, https://doi.org/10.1175/JCLI-D-11-00056.1.

——, and N. Henderson, 2013: Diagnostic computation of moisture budgets in the ERA-Interim reanalysis with reference to analysis of CMIP-Archived atmospheric model data. *J. Climate*, **26**, 7876–7901, https://doi.org/10.1175/JCLI-D-13-00018.1.

Smith, S. C., and D. Ubilava, 2017: The El Niño Southern Oscillation and economic growth in the developing world. *Global Environ. Change*, **45**, 151–164, https://doi.org/10.1016/j.gloenvcha.2017.05.007.

Todd, M., and R. Washington, 1999: Circulation anomalies associated with tropical-temperate troughs in southern Africa and the southwest Indian Ocean. *Climate Dyn.*, **15**, 937–951, https://doi.org/10.1007/s003820050323.

Van Zyl, J., H. J. G. Nel, and J. A. Groenewald, 1988: Agriculture's contribution to the South African economy. *Agrekon*, **27**, 1–9.

Washington, R., and A. Preston, 2006: Extreme wet years over southern Africa: Role of Indian Ocean sea surface temperatures. *J. Geophys. Res.*, **111**, D15104, https://doi.org/10.1029/2005JD006724.

Wehner, M. F., and Coauthors, 2014: The effect of horizontal resolution on simulation quality in the Community Atmospheric Model, CAM5.1. *J. Adv. Model. Earth Syst.*, **6**, 980–997, https://doi.org/10.1002/2013MS000276.

Williams, C. A., and N. P. Hanan, 2011: ENSO and IOD teleconnections for African ecosystems: Evidence of destructive interference between climate oscillations. *Biogeosciences*, **8**, 27–40, https://doi.org/10.5194/bg-8-27-2011.

Wiston, M., and K. M. Mphale, 2019: Mesoscale convective systems: A case scenario of the 'heavy rainfall' event of 15–20 January 2013 over southern Africa. *Climate*, **7**, 73, https://doi.org/10.3390/CLI7060073.

Wyrtki, K., 1975: El Niño—The dynamic response of the equatorial Pacific Ocean to atmospheric forcing. *J. Phys. Oceanogr.*, **5**, 572–584, https://doi.org/10.1175/1520-0485(1975)005<0572:ENTDRO>2.0.CO;2.

Zhang, Q., H. Körnich, and K. Holmgren, 2013: How well do reanalyses represent the southern African precipitation? *Climate Dyn.*, **40**, 951–962, https://doi.org/10.1007/s00382-012-1423-z.